Title
Cinnabar Alteration in Archaeological Wall Paintings: An Experimental and Theoretical Approach

Author
Neiman, Madeleine

Publication Date
2014

Peer reviewed|Thesis/dissertation

UNIVERSITY OF CALIFORNIA

Los Angeles

Cinnabar Alteration in Archaeological Wall Paintings:

An Experimental and Theoretical Approach

A thesis submitted in partial satisfaction of the requirements for the degree

Master of Arts in Conservation of Archaeological and Ethnographic Materials

by

Madeleine Kegelman Neiman

2014

ABSTRACT OF THE THESIS

Cinnabar Alteration in Archaeological Wall Paintings:

An Experimental and Theoretical Approach

by

Madeleine Kegelman Neiman

Master of Arts in Conservation of Archaeological and Ethnographic Materials

University of California, Los Angeles, 2014

Professor Ioanna Kakoulli, Chair

The red mineral pigment mercuric sulfide (HgS) was commonly employed in Roman wall paintings. Fresco artists of the period favored this pigment for its striking red color. Upon excavation and exposure to air and light, however, cinnabar pigmented surfaces recovered from archaeological contexts often proved unstable. Mural paintings colored with cinnabar that have been exposed in the open air frequently demonstrate a disfiguring, irreversible darkening of the surface. Traditionally, scholars have attributed this alteration to a light-induced phase change from red α-cinnabar to black β-cinnabar (meta-cinnabar) (Gettens *et al.* 1972). While this transformation has not been totally excluded, the prevailing view among conservation scientists is that chlorine plays a key role in the darkening process (Spring and Grout 2002, Keune and Boon 2005, Cotte *et al.* 2006, Cotte *et al.* 2008, Cotte *et al.* 2009 and Radepont *et al.* 2011), through the formation of light-sensitive mercury-chloride compounds, or as a catalyst in the photochemical redox of Hg(II)S into Hg(0) and S(0). Using laboratory-based experiments and thermodynamic modeling, this paper attempts to further clarify the mechanism(s) and kinetics of cinnabar alteration in fresco applications, specifically the role of light, humidity and chlorine ions. Additionally, it explores possible pathways, during or immediately following excavation, to inhibit or retard darkening of cinnabar pigmented fresco surfaces.

The thesis of Madeleine Kegelman Neiman is approved.

Christian Fischer

Mark Goorsky

Sergey Prikhodko

Magdalena Balonis-Sant

Vanessa Muros

Ioanna Kakoulli, Committee Chair

University of California, Los Angeles

2014

TABLE OF CONTENTS

LIST OF FIGURES

LIST OF TABLES

LIST OF EQUATIONS

Acknowledgements

I would like to express my sincere gratitude to my advisor Prof. Ioanna Kakoulli for her guidance, insight and encouragement. Her knowledge, wisdom and persistence have been essential in this work. I am also deeply grateful to the members of my thesis committee for their council, comments and suggestions. Their support and generosity with their time and knowledge has proved essential to my process of learning. I am very appreciative of the UCLA/Getty Conservation department who provided funding without which this research would not have been possible. I would finally, like to thank my cohort for their unending support in this endeavor.

CHAPTER 1: Introduction

Within the Roman World, mural paintings adorned both public and private spaces (Lehmann 1953, Clark 1991, Bussagli 1999). The walls of lararia (sacred place of affluent Roman homes), tombs and shop-façades were decorated with wall paintings depicting architectural vignettes and panoramic landscapes, as well as, scenes displaying daily life, historic events and mythic tales (Maiuri 1953, Ling 1991, Moormann 1993). These mural paintings serve as a cultural record of the ancient world; a testament to the technical and artistic skills of their creators as well as a visual chronicle of the society's religious, economic and social history. The study of archaeological wall paintings across the Mediterranean offers scholars an important point of entry into understanding ancient Roman culture and society.

While the excavation of ancient wall paintings has been a boon for archaeologists and art historians, the change in microclimate prompted by their unearthing induces – in many cases – new and accelerated degradation processes. Excavation disrupts the equilibrium of the burial environment spurring increased rates of decay. Once exposed, wall paintings are subject to chemical, mechanical and biological deterioration (Mora *et al*. 1984, Arendt 1991, Arnold 1991, Matteini 1991, Ciferri *et al.* 2000). The presence of salts, exposure to visible and ultraviolet light, pollution, microbiological activity and moisture, all contribute to the degradation of wall paintings generally and the pigmented surface in particular (Mora *et al*. 1984, Giovannoni *et al*. 1990, Arendt 1991, Arnold 1991, Matteini 1991, Dei *et al.* 1998, Ciferri *et al.* 2000, Daniels *et al.* 2004, Minopoulou 2009).

One of the most complex and challenging degradation processes in wall painting is color alteration. Shifts in hue, value or chroma, darkening or complete color transformation are not only visually disruptive and obscure the artist's intent, but they change the meaning and chemical stability of the painting. It is accepted, that the majority of the transformations and color changes in ancient painting

are principally induced by environmental exposure factors such as light, humidity, pH and microbial activity, assisted in some cases, by the action of different deteriogens such as sodium chloride (NaCl), often present as a soluble salt, deriving either from the constituent materials (wall, plaster, paint) as an impurity or as an external contaminant from the environment (Gettens 1966, Daniels 1987, Daniels *et al.* 2004, Giovannoni *et al.* 1990, Schiegl *et al.* 1992, Grout and Burnstock 2000). The most prevalent color transformations of ancient paint films (pigments/binding media systems) have been those containing photochemically-sensitive coloring materials including various 'lake' pigments made from the synthesis involving an organic dye and an inorganic substrate to form organometallic complexes, as well as mineral pigments such as orpiment (As_2S_3), realgar (α-As_4S_4), minium (Pb_3O_4) and cinnabar (HgS).

The darkening of cinnabar, in particular, has been one of the most common and puzzling color alterations in wall paintings. The phenomenon was first described and recorded in antiquity by Romans scholars that witnessed their paintings pigmented with cinnabar rapidly change from red to black. Pliny the Elder note during the first century A.D. in his work *Nauralis Historia* that "exposure to the light, either of sun or the moon, is injurious to the color" (Pliny 1929). Latin author Vitruvius – writing about Greek and Roman art and architecture during this same period – mentions in his book De Architectura, the application of a wax coating over areas painted with cinnabar to prevent it from darkening (Vitruvius 1960: VII:9). In modern times, cultural heritage professionals at the Roman site of Pompeii, Italy and at other archaeological sites with wall painting pigmented with cinnabar have reported the same phenomenon; red paint layers darken significantly after excavation (Gettens *et al.* 1986, Cotte *et al.* 2006).

1.1 Fresco and *secco* technique

In Classical antiquity, two different techniques were used for painting on walls: fresco and *secco*. Fresco technique refers to any painting executed on a moist calcium hydroxide (lime)-rich plaster layer. The

pigments are applied with water, and are fixed by the formation of a carbonate lattice during the setting of the lime based on Reaction 1.

$$\underset{\text{Slaked lime}}{Ca(OH)_2} + CO_2 \rightarrow \underset{\text{Carbonated lime}}{CaCO_3} + H_2O \uparrow$$

Reaction 1: The setting of lime is based on a chemical reaction between the calcium hydroxide and the carbon dioxide (CO_2) of the atmosphere.

Owing to the high alkalinity of the lime and the exothermic reaction during setting, only a small number of pigments are compatible with the fresco technique.

Secco technique involves no chemical reaction for the fixing of the pigments. As suggested by the etymology of the word ("secco" means "dry" in Italian), *secco* painting involves the use of dry plaster or whitewash, onto which the pigments are fixed by the use of a film-forming organic binding medium such as egg, siccative oil, gum and others. This technique is, therefore, not restricted to lime plasters. Plaster layers can involve also clay, gypsum, or calcium carbonate as the principle plaster binders. In many cases the painting is executed directly on the support (rock-cut surface, stone blocks).

During the Greek and Roman periods, fresco artists favored the use of cinnabar for its striking red color. While the pigment seems to withstand the high alkalinity of the slaked lime and remains generally unaffected during the setting, upon excavation and exposure to air and light, cinnabar often proves unstable. Archaeological mural paintings pigmented with cinnabar that have been exposed in the open air frequently demonstrate a disfiguring, irreversible darkening of the surface. Though this is an ancient phenomenon, the mechanisms and kinetics of the transformations involved in the alteration of cinnabar in archaeological wall paintings still provide an analytical challenge that needs further and systematic investigation.

1.2 Scope of research

Building on previous scholarship on the alteration of cinnabar in bulk geological samples (McCormack 2000), egg-tempera and oil-based paint films in fine art paintings (Feller 1967, Gettens *et al.* 1986, Daniels 1987, Spring and Grout 2002, Keune and Boon 2005 and Radepont 2013) and Byzantine wall paintings (Pique *et al.* 2007; Kakoulli and Fischer 2009; Sotiropoulou *et al*. 2008, Radepont *et al.* 2011) as well as the few studies on archaeological wall paintings (Cotte *et al.* 2006, Cotte and Susini 2009, Radepont *et al.* 2011, Radepont 2013), this paper attempts to further clarify the mechanism(s) of cinnabar alteration in fresco applications, specifically the role of light and chlorine ions, through laboratory-based experiments and thermodynamic modeling. The aim is to understand better the transformations involved as a means to aid conservators in determining what steps may be taken during or immediately following excavation of wall paintings pigmented with cinnabar to slow down, mitigate or avoid the further darkening of the paint layer.

1.3 Outline of research

The research is divided into the following seven chapters:

CHAPTER 1 **Introduction:** This chapter provides the background and scope of the research of this study.

CHAPTER 2 **Literature review:** A compilation of published and unpublished literature on cinnabar alteration including all theories proposed.

CHAPTER 3 **Materials and Methods:** The chapter describes the laboratory simulations of archaeological wall painting pigmented with cinnabar in a fresco application, and the method employed to artificially induce alteration of cinnabar using sodium chloride (NaCl) and light (in air). This is followed by an account of two proposed methodologies for inhibiting this alteration process. The remainder of the chapter is devoted to a detailed description of the application of a multi-

analytical approach at multiple scales for the characterization of the alteration phases and understanding of the mechanisms and kinetics of the alteration.

CHAPTER 4 **Results:** Recounts the data resulting from the analysis of alteration layer induced on artificially aged fresco mock-ups as well as bulk powder samples; specifically, the colorimetric, chemical and morphological changes observed. The chapter additionally described the efficacy of the preventative conservation methodologies employed to inhibit alteration.

CHAPTER 5 **Thermodynamic modeling:** Describes computed calculations and prediction models for the alteration phases of cinnabar created using GEMS-PSI: Gibbs Energy Minimization Software.

CHAPTER 6 **Discussion**: This chapter compares the experimental results of this study with alteration phases predicted through thermodynamic modeling as well as those identified in previous studies in an attempt to determine what phase(s) is (are) responsible for the darkening of cinnabar. Proposed mechanisms for this alteration process are additionally explored.

CHAPTER 7 **Conclusion**: Provides a summary of the findings of this study as well as preventive conservation recommendations for cultural heritage professionals charged with the care of archaeological wall paintings.

CHAPTER 2: Literature Review

Traditionally, scholars have attributed cinnabar alteration to a light-induced conformational change from red α-cinnabar (HgS trigonal) to black β-cinnabar (meta-cinnabar, HgS cubic) (Feller 1967, Gettens *et al.* 1972, Daniels 1987, Spring and Grout 2002 and Grout and Burnstock 2000). Early analysis of the altered material only identified Hg and S, leading to the assumption that a shift in the crystal structure was responsible for the color change. However, the more recent use of highly sensitive microanalytical techniques, including Raman spectroscopy, as well as, synchrotron-based spectromicroscopies such as x-ray diffraction (SR-μXRD) and x-ray absorption near edge structure (SR-μXANES), has not supported this hypothesis. To date, metacinnabar has only been identified within altered cinnabar on one cultural heritage object; Istudor (2007) detected metacinnabar during an examination of wall paintings from a sixteenth century Sucevita church. Additionally, a review of the geochemical literature suggests a transformation from α-cinnabar to β-cinnabar requires the application of significant thermal energy; α-cinnabar must be heated to an excess of 381°C to cause a phase change (Dickson and Tunell 1959).[1] This stands in contrast, to anecdotal and empirical accounts that describe cinnabar alteration under ambient conditions (McCormak 1997, McCormak 2000, Radepoint 2013 and Cotte *et al*. 2006). While the theory is largely considered outmoded, it continues to be cited within the literature as a possible means of explaining the blackening of cinnabar (Béarat *et al.* 2013).

More recently, conservation science has drawn on geochemical research showing that halogen impurities, in particular chlorine (Cl), are responsible for the photosensitivity of cinnabar (McCormak

[1] The presence of zinc or iron has been shown to reduce the temperature of transformation, to 204°C and 305°C respectively. While substantially lower, the temperature required to induce this phase change still remains quite high (Dickson and Tunell 1959).

1997, McCormak 2000, Davidson and Willsher 1981).[2] McCormak *et al.* (1991) and McCormak (1997) demonstrated that exposure of cinnabar to halide solution will induce photosensitivity of the ore. McCormak (2000) examined samples of naturally occurring photosensitive and non-photosensitive cinnabar gleaned from mines across the globe using microprobe analysis; the study found that only the photosensitive ores contained chlorine. Analysis of cultural heritage materials has shown a similar correlation between the presence of chlorides and blackening of cinnabar in oil and tempera canvas paintings, as well as, frescoes. In these studies, scholars have identified the presence of mercury chloride-containing compounds in the blackened areas. (Spring and Grout 2002, Keune and Boon 2005, Cotte *et al.* 2006, Cotte *et al*. 2008, Cotte *et al.* 2010, Radepont *et al.* 2011, Radepont 2013).

While conservation scientists now largely agree that the chlorine plays a key role in the alteration process, the specific mechanism by which this occurs remains ambiguous. Scholars have posited two possible pathways by which chlorine might provoke a light-induced alteration. In the first, chlorine reacts with cinnabar to form various light-sensitive mercury-chloride and mercury-sulfochloride compounds (Spring and Grout 2002, Cotte *et al.* 2006, Cotte *et al.* 2008, Cotte *et al.* 2010 and Radepont *et al*. 2011). Analysis of blackened cinnabar on cultural heritage materials has identified the presence of calomel (Hg_2Cl_2), mercuric chloride ($HgCl_2$) as well as $Hg_3S_2Cl_2$ polymorphs including corderoite (α-$Hg_3S_2Cl_2$), β-$Hg_3S_2Cl_2$ and kenhsuite (γ-$Hg_3S_2Cl_2$) (Table 1). The presence of such compounds could certainly alter the color of the surface as Cotte *et al.* (2006) and Radepont *et al.* (2011) suggest; colomel and corderoite in particular are grayish in color. To our knowledge, however, there is no known mercury chloride-containing compound that would account for the black color observed. A second pathway for the transformation is described by Keune and Boon (2005) who proposed that chlorine serves to catalyze the photochemical redox of Hg(II)S into Hg(0) and S(0). They posit that nonparticles of colloidal

[2] While chlorine has been the most thoroughly explored, other halogens, namely iodine have also been shown to trigger the blackening of cinnabar.

Hg(0) – metallic mercury – deposited on the remaining intact HgS surface result in the blackened appearance. The presence of Hg-Cl compounds is explained by the subsequent reaction of Hg(0) with excess chloride ions. It should be noted, however, while they were able to identify mercury-chloride containing compounds, the presence of metallic mercury could not be conclusively proven.

The formation of a sulfate-based compound, more specifically gypsum, has also been suggested as a possible source of darkening on cinnabar pigmented frescoes. The presence of black gypsum crusts[3] on a variety of calcareous surfaces including limestone, marble and wall paintings due to SO_2 pollution is well documented within the conservation literature (Gauri *et al.* 1999, Ausset *et al*. 1992, Fassina 1992, Tennikat 1994, Charcola and Ware 2002, Charola *et a*l. 2007, Toniolo *et al.* 2009, Doehne and Price 2010). Gypsum has been detected in areas of altered cinnabar on fresco samples recovered from Pompeii (Cotte *et al*. 2006, Radepont *et al.* 2011 and Radepont 2013) and Santa Maria Church in Northern Spain (Perez-Alonso 2006). However, as noted above, cinnabar alteration has been observed on a range of artworks including oil and tempera paintings as well as on the ore itself. The presence of calcium carbonate is not required for cinnabar to darken. Therefore, while black gypsum crusts on some cinnabar pigmented wall paintings have likely contributed to the darkening, they cannot be considered responsible for the light-induced blacking of cinnabar.

[3] In the presence of moisture, sulfur dioxide in the atmosphere dissolves in the water to form sulfurous acid (Guari et al. 1989). This sulfurous acid then combines with oxygen to form sulfuric acid which is then deposited on the stone surface. The sulfuric acid and calcareous stone react creating a calcium sulfate or gypsum crust. While gypsum itself is light white or colorless, soot and dust particles, which are incorporated into the curst as it forms cause it to appear black.

Table 1. Previously identified compounds in altered cinnabar on cultural heritage materials

Compound	Color	References
Calomel (Hg_2Cl_2)	White	Spring and Grout 2002: Raman spectroscopy
		Keune and Boon 2005: (secondary ion mass spectrometry – SIMS); likely, but can not be definitively identified.
		Cotte *et al.* 2006: μXANES
		Cotte *et al.* 2008: μXANES
		Cotte *et al.* 2009: μXANES
		Maguregui *et al.* 2009: Raman spectroscopy
		Radepont *et al* 2011: μ-XRD, μXANES
		Radepont 2013: μ-XRD, μXANES
Mercuric Chloride ($HgCl_2$)	White to Light Gray	Keune and Boon 2005: SIMS
Corderoite (α-$Hg_3S_2Cl_2$),	Orangey Pink, Grayish Purple	Keune and Boon 2005: SIMS
		Cotte *et al.* 2006: SR-μXANES
		Cotte *et al.* 2008: SR-μXANES
		Cotte *et al.* 2009: SR-μXANES
		Radepont *et al* 2011: SR-μXRD, SR-μXANES
		Radepont 2013: SR-μXRD, SR-μXANES
β-$Hg_3S_2Cl_2$	Unknown	Radepont 2013: SR-μXRD, SR-μXANES
Kenhsuite (γ-$Hg_3S_2Cl_2$)	Yellow	Radepont *et al* 2011: SR-μXRD, SR-μXANES
		Radepont 2013: SR-μXRD, SR-μXANES
Gypsum ($CaSO_4 \bullet 2H_2O$)	Clear to White	Cotte *et al.* 2006: SR-μXANES
		Radepont *et al* 2011: SR-μXRD, SR-μXANES
		Radepont 2013: SR-μXRD, SR-μXANES
		Perez- Alonso 2006: Raman spectroscopy
Metacinnabar (β-HgS)	Black	Istudor 2007: Raman spectroscopy

The source of chlorine within cinnabar pigmented archaeological fresco paintings, as well as, the timing of its introduction remains obscure. Mercury-chloride and mercury-sulfochloride compounds, including corderoite and calomel, have been found to coexist with cinnabar in geological contexts (Radepont 2013: 22). Chloride contamination might have also occurred during processing of the pigment prior to use. The Roman architect Vitruvius wrote in the first century AD: "When the lumps of ore are dry, they are crushed in iron mortars and repeatedly washed and heated until impurities are gone and the colors come" (Vitruvius 1960). Cotte *et al.* (2006) has suggests that Punic wax, a protective coating applied to fresco surfaces in antiquity might have served as the source of chlorine. Pliny the Elder wrote in his work *Nauralis Historia*: "Punica wax is made this way: yellow beeswax is often exposed to air for a long time, then it is boiled in water from high sea, to which added nitre. Then, wax bloom is removed with a spoon, e.g. the whitest part, and is poured into a pot containing a bit of cold water, this part is

boiled again in seawater, an then the vas is cold" (Pliny 1929). That Pliny the Elder recognized the problem of cinnabar alteration in antiquity writing that "exposure to the light, either of sun or the moon, is injurious to the color" supports the idea that, at least in some cases, chlorine present prior to burial (Pliny 1929). However, it is similarly possible that chlorine-containing compounds within the soil or groundwater have served as the source of contamination.

CHAPTER 3: Materials and Methods

3.1 Preparation of fresco block mock-ups

Fresco mock-ups were fabricated by combining commercial calcium hydroxide (lime putty), Carrera marble dust (0.2-0.6 mm) and deionized water in a 1:3:1 volumetric ratio.[4] This dense mortar was decanted into custom-made stainless-steel molds (5cm x 5cm x 2cm) and allowed to dry for approximately 2 hours. The damp surface was then painted with a fluid mixture of 2:1 w/v natural cinnabar and deionized water. Blocks were subsequently left to dry in the dark at under ambient conditions (23-26° C and ~35-55% RH) for one week; at which time, they were unmolded and allowed to carbonate for not less than 6 weeks.

3.2 Accelerated artificial discoloration

In order to artificially reproduce the alteration observed in archaeological frescoes, laboratory-produced mock-up blocks were first infused with sodium chloride solutions of different molarities via capillary action and subsequently exposed to light.

3.2.1 Introduction of saline solutions

The mock-ups were infused with either a low (0.1M) or a high concentration (5M) of sodium chloride solution replicating the extremes of salinity, which might be found within a fresco unearthed from an archaeological context. Sodium chloride solutions were introduced via capillary impregnation. For this experiment, a single layer of glass beads was spread across the base of a petri dish and the fresco mock-up blocks were placed on the beads with the paint surface down. The salt solution was pipetted into the dish until level with the painted surface, allowing the salt solution to be transferred through the block by

[4] Materials and proportions are consistent with known standards for the fabrication of plaster supports during the Roman period. Technical analysis of frescoes has demonstrated that cinnabar was typically applied over lime bulked with marble dust rather then river sand- which was found in other, more commonly employed, less valuable pigments (Béarat 1996).

capillary action. Blocks were left in contact with the saline solution for approximately 12 hours. The pH of the saline solution at the beginning and the end of the infusion period was recorded with a Merck© pH strip. An indicator strip was dipped into the solution at hour 0 and at hour 12.

3.2.2 Light exposure

The mock-up blocks were subsequently exposed to sunlight. Published literature attributes the cinnabar darkening to ultraviolet and visible light wavelengths. However, no evidence-based study has resolved which exact part of the electromagnetic radiation is responsible for the alteration. Therefore, a choice was made to recreate conditions similar to those found in the field. The mock-ups were exposed to sunlight under ambient condition. Fresco blocks were placed onto a windowsill at the UCLA/Getty training laboratories at the Getty Villa in Malibu, CA and exposed to sunlight for ten weeks. Light levels, temperature and relative humidity (RH) were recorded indicating variations within and across the days of exposure ranging between 0-4500 lux, 0-500 µW/lm, 23-36 °C and 35-55% RH. The set-up avoided contamination by atmospheric pollutants or weathering of the sample surfaces, which could have affected the experimental results.

3.3 Desalination process

Previous work has shown that the alteration is irreversible. Once the surface of the cinnabar has blackened, it cannot be reconverted to its pervious red state. Therefore, this study has focused on determining what steps, if any, could be taken to inhibit, curtail or slow down the alteration process. Two primary strategies were explored: (1) varying the moment of light exposure during the drying process or (2) chlorine ion reduction.

Anecdotal accounts have suggested that moisture may enhance or accelerate the rate of cinnabar darkening (Dreyer 1938 and McCormak *et al.* 1991). In order to explore how varying the moment of light exposure during the drying process would impact the extent of alteration – specifically

to check whether low moisture levels at the time of light exposure would retard the alteration- mock-ups were divided into two groups. **Group A** was exposed to light while wet; blocks were placed into the sun immediately upon their removal from a salt solution. **Group B** was dried prior to light exposure; mock-ups were allowed to dry in the dark under ambient conditions until they came to a constant weight before they were exposed to light.

McCormak (2000) notes that geological specimens of cinnabar with an average over 0.05 Cl wt% are photosensitive; those with an average below 0.01 Cl wt% are not photosensitive. To test this hypothesis, after the exposure of the blocks to the saline solutions, the chlorine ions were removed from the salt-contaminated fresco via a desalination process. The goal was to place the Cl wt% below this threshold prior to light exposure. Mock-ups were removed from the salt solution and allowed to partially dry in darkness under ambient conditions for three days. At end to this period samples were cool to the touch while continuing to loose weight. As most fresco paintings are often recovered from damp soil, they tend to have relatively high water content. Allowing samples to partially dry replicates this environment. Subsequently, samples were desalinated with cellulose poultices (Figure 1). Arbocel® BC 200 and deionized water was combined in a 1:5 ratio to form a paste and gently pressed against the surface of the block creating a 1 cm thick compress. It should be noted that a permeable layer of thin Japanese tissue (MN-1 Tencucho 5 g/m^2) was placed at the interface between the poultice and fresco mock-up to prevent cellulose fibers from adhering to the surface of the block. The blocks were then allowed to stand until the cellulose fibers were dry to the touch; approximately 72 hours. The poultice was then removed and the conductivity of the rehydrated poultice was measured as an indication of the salt (NaCl) extracted. This process was repeated five times, after which the mock-ups were exposed to light as described above.

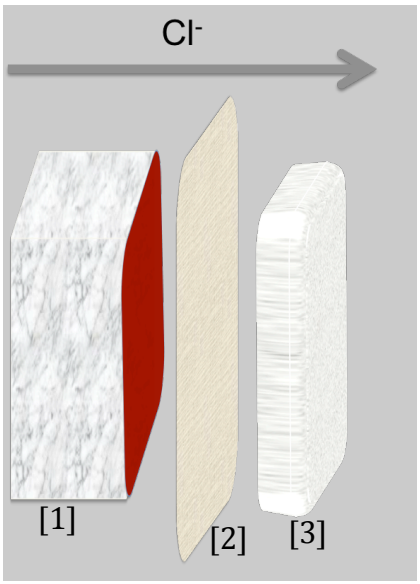

Figure 1: Schematic representation of the desalination process. Fresco mock-ups [1] were desalinated (to remove the Cl^- ions) using cellulose fiber-based compresses [3]. A thin Japanese tissue (MN-1 Tencucho 5 g/m^2) barrier layer [2] was placed between the mock-up and the poultice. Arbocel® BC 200 and deionized water combined in a 1:5 ratio to form a paste was then gently pressed over the tissue creating a 1 cm thick compress across the block [3]. As the cellulose fibers dried, Cl^- ions present within the block were drawn out of the block and into the poultice.

3.4 Artificial accelerated weathering of pigment powders

As a point of comparison, samples of powdered pigment were also artificially weathered through exposure to 0.1M and 5M saline solutions and exposure to light. Cinnabar was combined with saline solution at a 1:25 w/v ratio, mixed thoroughly and allowed to stand for approximately 12 hours in the dark. At the end of this period, the saline solution was decanted and approximately 0.25g of cinnabar was spread onto the surface of each glass slide. In order to disambiguate the impact of moisture on the alteration process, the RH of the environment was controlled during the drying process. Samples were alternately housed in inert polypropylene containers with silica gel conditioned to 5%, 50% or 70% relative humidity (RH). Finally, samples were placed directly onto the windowsill the Getty Villa in Malibu, CA for a period of 21 days. Light levels and temperatures during this period varied within and across the days, ranging between 0-4500 lux, 0-500 µW/lm and 23-36 °C.

3.5 Sample preparation

Stratigraphic polished cross sections were prepared by embedding samples in Bio-Plastic® polyester resin and hardener.[5] Upon hardening, samples were ground using Buehler silicon carbide grinding papers from 240 to 1200 grit. Cross sections were subsequently polished on a Leco® GP-25 polishing turntable using 6 µm and 1 µm diamond paste thinned with isopropanol[6] on Buehler® MasterTex and appropriate polishing cloths.

3.6 Characterization methods

3.6.1 Ultraviolet/Visible light/Near Infrared (UV/Vis/NIR) reflectance spectroscopy and colorimetry

Color measurements were preformed using the FieldSpec3® 3 by Analytical Spectral Devices Inc (ASD), with high spectral resolution (3 nm @ 700 nm and 10 nm @ 1400/ 2100 nm) and wide spectral range between 350-2500 nm. Spectro-colorimetric measurement allowed quantification of incident and reflected radiation intensities, which roughly equates to human color perception (Radepont 2013: 121 and Johnston-Feller 2001: 34-35). Change in color (ΔE*) was calculated with the following formula defined in 1976 by the CIE (Commission Internationale de l'Eclairage):

$$\Delta E^* = [(\Delta L^*)2 + (\Delta a^*)2 + (\Delta b^*)2]^{1/2}$$

Equation 1. Change in color (ΔE*) where ΔL* describes the change in luminance, Δa* the change in green/red components and Δb* the change in blue/yellow components.

3.6.2 Optical microscopy

The extent of paint layer discoloration and pigment alteration was evaluated at first using optical microscopy (OM) including stereomicroscopy (STM) and digital microscopy (DM). Changes to the bulk

[5] Bio-Plastic® [Aldon Corp, Avon, NY] is a polyester resin which has been blended with methacrylate monomers in a styrene solvent. The speed of curing is increased with a methyl ethyl ketone catalysis (solution also contains: dimethyl phthalate, 2,4-trimethyl-1,3-pentaediol diisobuterate, hexylene glycol, methyl ethyl ketone, water, hydrogen peroxide). It is important to note the absence of chlorine- commonly found in the epoxy resins often employed in conservation- which would otherwise interfere with the ability to examine analyze the role of chlorine in the alteration process which in the focus of this work.

[6] Isopropanol was employed as an alternative to water in an effort to limit the loss of any sodium chloride or mercury chloride salts.

surface of the blocks were captured using Nikon D90 Digital SLR camera allowing for qualitative assessment of color changes within and between blocks during aging. Images were recorded a with a color reference panel and color corrections made, as necessary, using Adobe Photoshop to ensure the colorimetric fidelity of the image.

Digital microscopy provided higher resolution imaging of mounted (as polished sections) and un-mounted (small fragments without any preparation) samples. Both polarized light microscopy and digital microscopy allowed enhanced visualization of individual blackened particles. Photomicrographs were taken with an Olympus BX51 polarized light microscope and under a KEYENCE VHX-1000 digital microscope at 20x, 50x, 100x, and 200x magnification.

3.6.3 X-Ray Fluorescence (pXRF) spectroscopy

For elemental characterization, the Thermo Scientific Niton® XL3t Series GOLDD™ technology handheld portable XRF was used, with a silver anode and silicon drift detector. Readings were taken with an 8 mm diameter spot size in both Soil Mode and Mining Mode for 120 seconds for each measurement. In situ study of the samples with this technique gave semi-quantitative information regarding the relative concentrations of chlorine in the sample and complemented other microanalyses.

3.6.4 Scanning Electron Microscopy (SEM) and Energy Dispersive X-Ray Spectroscopy (EDS)

As the degradation layer is typically quite thin (several micrometers or less), scanning electron microscopy enabling high spatial resolution was used. Scanning electron microscopy (SEM) was preformed with a FEI Nova™NanoSEM 230. To avoid the necessity of carbon or metal sputtering, a low vacuum mode (variable pressure) was applied during the analysis. Morphological characteristics of the surface and topographical contrast were recorded with the secondary electron detector (SE) using the Low Vacuum Detector (LVD). Compositional contrast was assessed with the backscattered electron

detector (BSE) using a gaseous analytical detector (GAD) and spatially resolved elemental analysis was performed with a Thermo Scientific NORAN System 7 energy dispersive x-ray spectrometer (EDS).

Samples were first examined non-invasively at low vacuum, so as not to damage, dehydrate, or alter the materials. Polished cross-sections were also analyzed with SEM-EDS for spatially resolved inter- and intra-layer visualization and characterization. Elemental spectra and maps of characteristic X-ray photon emissions were acquired using EDS. The analysis of well-polished surfaces was crucial for more precise quantitative measurements because of the shallow probing depth of electrons interacting with the surface. In addition, flat surfaces minimize the deflection of BSE in different directions, maximizing the collection of electrons by the detector located symmetrically about the incident beam of electrons. EDS spot analysis enabled comparisons of peak intensities, providing data regarding relative concentration of the chlorine (Cl) and sulfur (S) found in the specimen, and elemental mapping of certain areas provided a visual of the profile distribution of these elements.

3.6.5 Powder X-ray Diffraction (XRD)

Powder X-ray Diffraction (XRD) provided characterization of the crystal phases within the degradation products observed on the artificially weathered mock-ups. This technique served as a means to access samples for the presence of new compounds as well as conformational changes within the cinnabar molecule; specifically, the occurrence of mercury chloride-containing salts or HgS polymorphs. For the analysis, a few particles of the area of interest were mounted on a glass spindle using Apiezon high vacuum grease and analyzed using a Rigaku R-Axis Spider X-ray diffractometer. XRD spectra were recorded at 50 kV/40 mA using a Cu-Kα target for 900 seconds. Bulk powder samples were run for 1,200 seconds. XRD data was processed and matched against reference spectra from the International Center for Diffraction Data (ICDD) files using the JADE, v8.2 software from Materials Data Inc.

CHAPTER 4: Experimental Results

4.1 Discoloration of fresco wall paintings mock-ups

Photographs and color measurements taken of the simulated fresco blocks pigmented with cinnabar and infused with saline solution over the ten week period of light exposure capture the swift and dramatic discoloration of red cinnabar into grey/black (Figure 2C[I-VIII] - F[I-VIII]). In the presence of 0.1M of NaCl, the color change of the surface was visible within the first 6 hours of light exposure both when dried in the light and when dried in the dark (and then exposed to light) (Figure 2C[I-VIII] & E[I-VIII]). Similar patterns were observed also for the blocks infused with 5M NaCl (Figure 2D[I-VIII] & F[I-VIII]). Generally, it appears that the alteration began at the edges of the samples and progressed inwards. After 70 days, the fresco simulated blocks showed significant discoloration; the previously bright red surface became muted and mottled (Figure 2C[I-VIII] - F[I-VIII]). A light lilac-gray alteration was visible in select areas across the surface and the edges were a deep gray/black. The color values of these transformations are tabulated in Table 6. Minor alteration was also observed on the surfaces of the control block (Figure 2A[I-VIII]). Those placed into the light with no treatment or having been wet only with DI H_2O exhibited a fine gray haze covering much of the surface (Figure 2B[I-VIII]). The intensity of surface blackening did not increase with the molarity of the solution; blocks impregnated with 0.1M and 5M solutions show approximately the same level of darkening. However, both the color and surface morphology of blocks wet with a 5M NaCl solution were impacted by the formation of white halite crystals (Figure 2D[I-VIII] & F[I-VIII]).

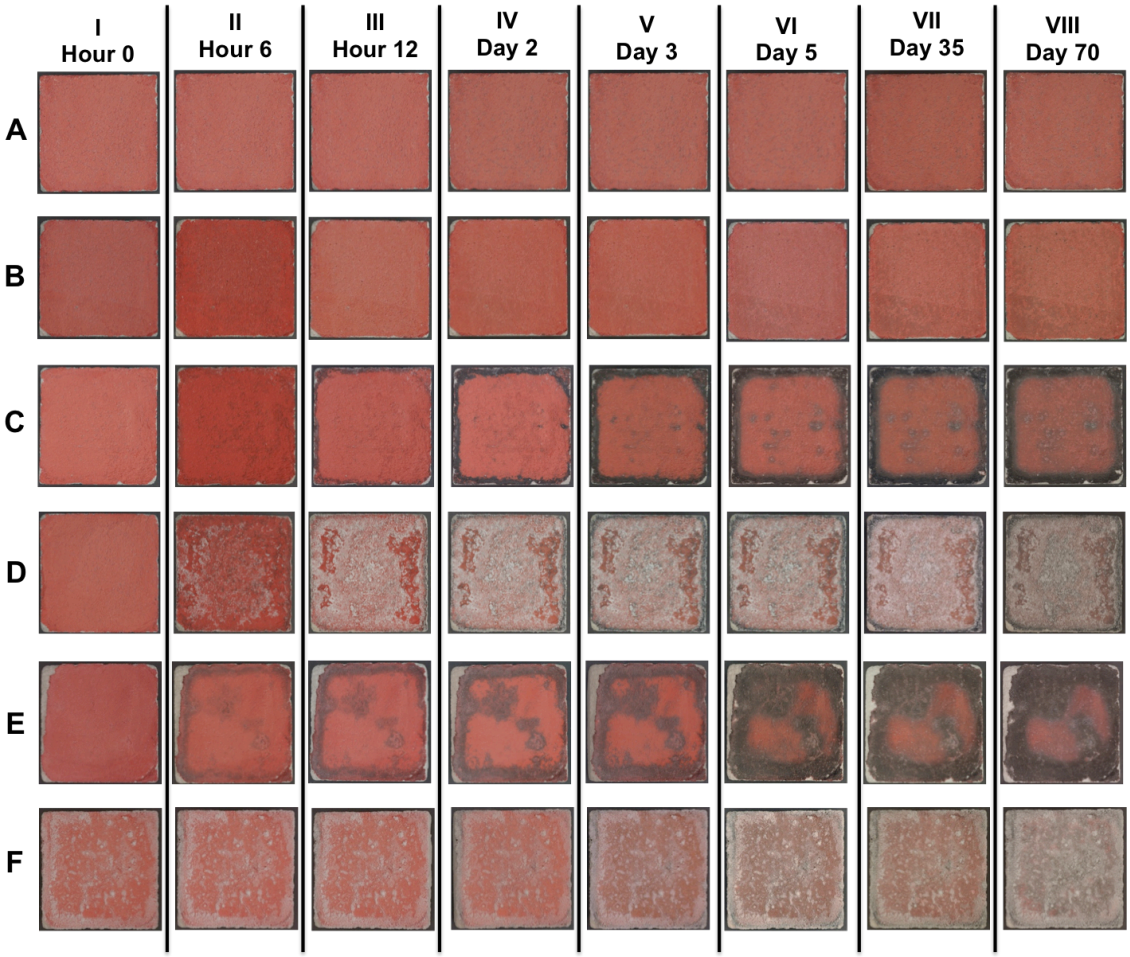

Figure 2. Images of fresco wall painting mock-ups captured during the 10-week-period (70 days) of light exposure on a windowsill at the Getty Villa in Malibu, CA. The blocks were infused with saline solution in order to induce alteration of the surface upon subsequent light exposure with the exception of A[I-VIII] and B[I-VIII] that act as control samples. **A[I-VIII]:** No exposure to any solution prior to placement in light; **B[I-VIII]:** Exposed to DI H_2O alone, dried in the light; **C[I-VIII]:** Exposed to 0.1M NaCl solution, dried in light; **D[I-VIII]:** Exposed to 5M NaCl solution, dried in light, **E[I-VIII]:** Exposed to 0.1M NaCl solution, dried in dark prior to placement into light exposure; **F[I-VIII]:** Exposed to 5M NaCl solution, dried in dark prior to light exposure. Images were taken at different time intervals: **I**=Hour 0; **II**=Hour 6, **III**=Hour 12, **IV**=Day 2; **V**=Day 3; **VI**=Day 5; **VII**=Day 35 and **VIII**=Day 70.

Table 2. Color change of bocks over 70 days of light exposure captured with UV/Vis/NIR Spectrometer. Block designations A-F refer image displayed in Figure 2

Block	Pre-Experiment Values			Value After 70 Day Aging			ΔE*
	L*	a*	b*	L*	a*	b*	
A	66.72	27.97	16.183	63.85	24.89	12.77	5.40
B	62.43	28.99	15.84	61.35	26.68	14.44	2.98
C	60.61	30.81	18.73	61.48	25.13	13.31	7.90
D	62.27	29.81	18.34	73.55	6.90	.90	30.93
E	69.68	9.15	14.18	76.71	3.10	.86	7.21
F	66.63	26.03	15.14	74.43	3.37	.92	27.87

Microscopic optical examination of cross sections from darkened areas shows that, while the color change observed is intense, the alteration is highly superficial; it only occurs at the surface and subsurface ranging form 5 to 20 μm in depth (Figure 3). Examination of the surface cross section at high magnifications suggests that variation in color observed at the macroscopic level is a product of both the extent to which an individual particle has altered and the density of altered particles. Blackening of individual particles begins along the edges and moves inwards with total color discoloration of the smaller particles (Figure 4). The overlay of a fine black degradation layer across the intact red substrate causes the particle appear a deep maroon. The relative proportion of red to black particles has a similar effect (Figure 5). In areas with a high concentration of black particles, the surface appeared more gray/black (Figure 5C); whereas, areas with a greater mixture of red and black particles, the surface takes on a hazy grayish-purple (Figure 5D).

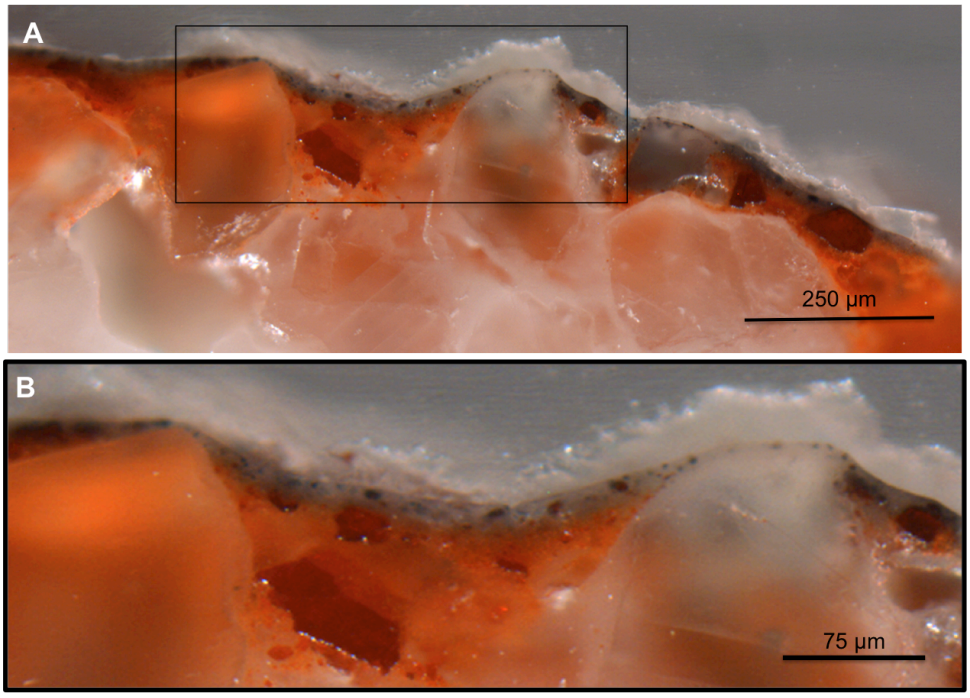

Figure 3. Cross section removed from a blackened area of fresco block impregnated 5M NaCl solution, dried in dark and subsequently exposed to light for 70 days. (A) The fresco is comprised of four discrete layers; (1) the white $CaCO_3$ fresco substrate prepared by combining $Ca(OH)_2$ with marble dust aggregate, (2) red HgS pigment, (3) altered/blackened particles and (4) surface crust of halite crystals. (B) Examination in cross section shows the alteration layer to be highly superficial; it only occurs at the surface and subsurface of approximately 5 to 20 μm depth.

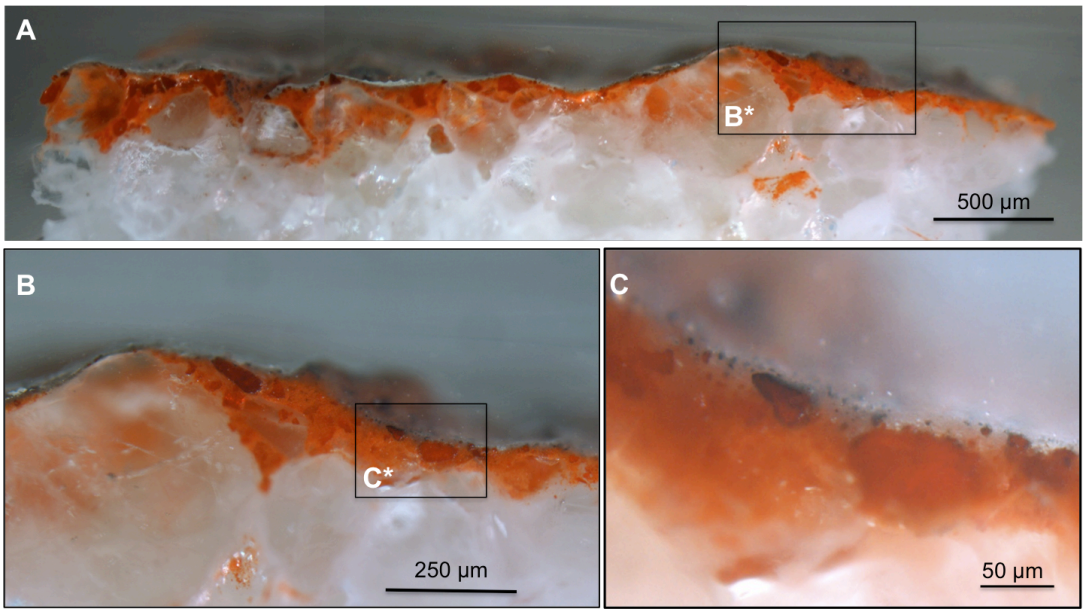

Figure 4. (A) Cross section removed from blacked section of fresco block impregnated 0.1M NaCl solution and exposed to light for 70 days. (B) Very thin alteration layer; the particles at the surface has just begun to blacken. (C) Highly magnified image of the altered surface shows that blackening of individual particles begins along the edges.

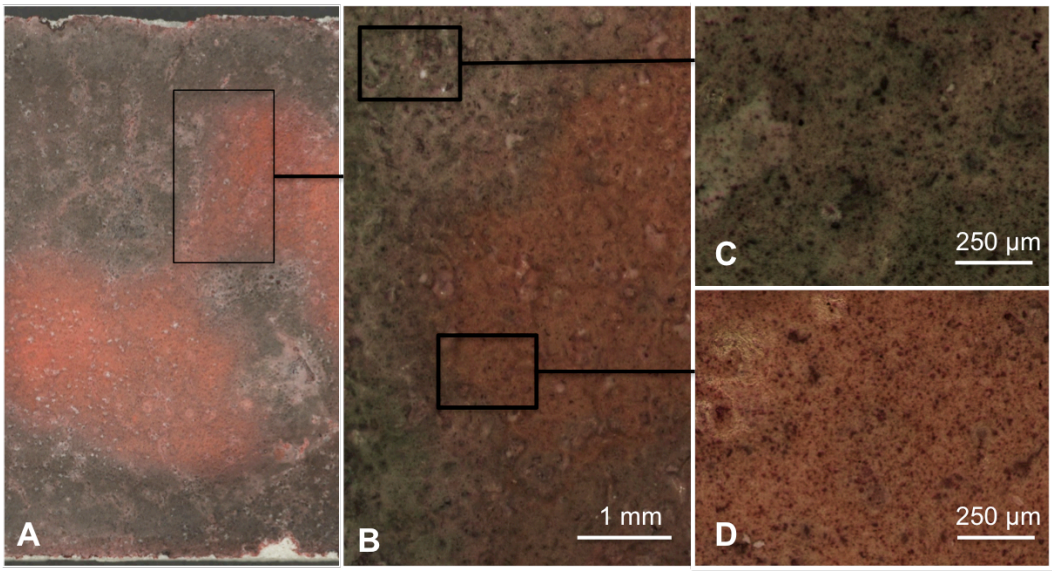

Figure 5. (A) Central third of a fresco block impregnated 0.1M NaCl solution, dried in the dark and subsequently exposed to light for 70 days. The photograph shows the variation in color observed when examining the alteration layer at a macroscopic level; the surface ranges from a dark pink to a soft purple-gray to a deep gray-black. (B) Magnified image of altered surface. Microscopic examination of reveals the color change relates to the intensity relative proportion of red to black particles. (C) Areas with a high concentration of black particles the surface appeared gray/black. (D) Areas with a greater mixture of red and black particles the surface takes on a hazy grayish-purple.

4.2 Discoloration of pigment powders

Examination of the powder samples of cinnabar showed similar results (Table 3). Only the cinnabar powders exposed to saline solution, light and relatively high RH (between 50 and 75%) showed evident color change from red to black. Cinnabar treated with DI H_2O remained red regardless of light exposure, and cinnabar kept in the dark remained red regardless of exposure saline solution. Cinnabar powders exposed 0.1M saline solutions, light and RH between 50 and 75% (Figure 6C[I-IV]) as well as those exposed to 5M NaCl solution, light and RH at ~50% (Figure 6D[I-IV]) showed severe blackening. The pattern of alteration in the 0.1M NaCl is uniform and spreads homogeneously over the entire surface of the particles. In the 5M NaCl, the blackening is speckled with spots of intense blackening surrounding the halide crystals. The artificially weathered samples (exposed to saline solutions) and placed in a low RH environment (~ 5%) showed no color change over the 21-day-period of light exposure (Figure 6A[I-IV]). In contrast those exposed to a high RH environment (~50-75%) and light demonstrated intense and significant blackening Figure 6C[I-IV] & D[I-IV]).

Table 3. Presence or absence alteration observed in cinnabar powders upon exposure to DI H_2O, 0.1M NaCl solution or 5M NaCl solution as impacted by light exposure and relative humidity (highlighted cells displayed color change)

Solution Salinity	RH (± 5%)	Light Exposure	Visible Alteration
DI H_2O	5	No	No
DI H_2O	5	Yes	No
DI H_2O	50	No	No
DI H_2O	50	Yes	No
DI H_2O	75	No	No
DI H_2O	75	Yes	No
0.1M	5	No	No
0.1M	5	Yes	No
0.1M	50	No	No
0.1M	50	Yes	Yes
0.1M	75	No	No
0.1M	75	Yes	Yes
5M	50	No	No
5M	50	Yes	Yes

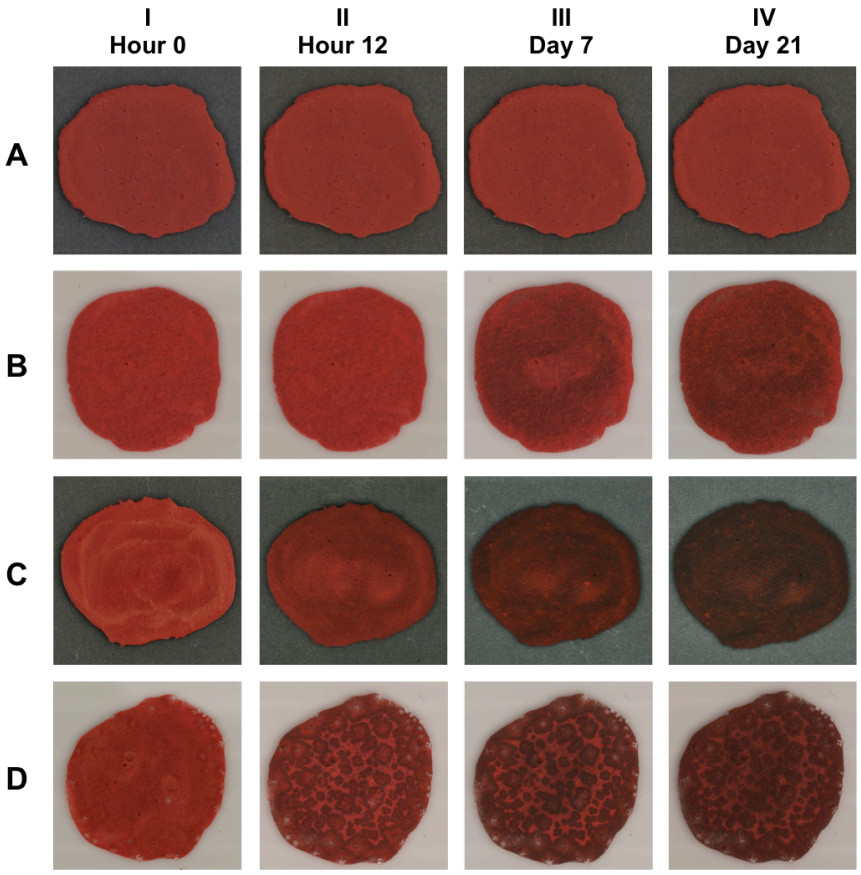

Figure 6. Images of bulk cinnabar powder captured during the 21-day-period of light exposure in a windowsill at the Getty Villa in Malibu, CA. **A[I-IV]:** Exposed to 0.1M NaCl solution and kept at 5% RH; **B[I-IV]:** Exposed to 0.1M NaCl solution and kept at 50% RH; **C[I-IV]:** Exposed to 0.1M NaCl solution and kept at 70% RH; **D[I-IV]:** Exposed to 5M NaCl solution and kept at 50% RH.

4.3 Change in morphology

High-resolution SEM imaging of the darkened particles indicated a change in their morphology; the black particles display a distinct amorphization when compared to the characteristic rhombohedral/tabular habit of the red control particles (Figure 7A & C). Figure 7B & D, shows the change in the particles morphology after exposure to 0.1M NaCl solution and light.

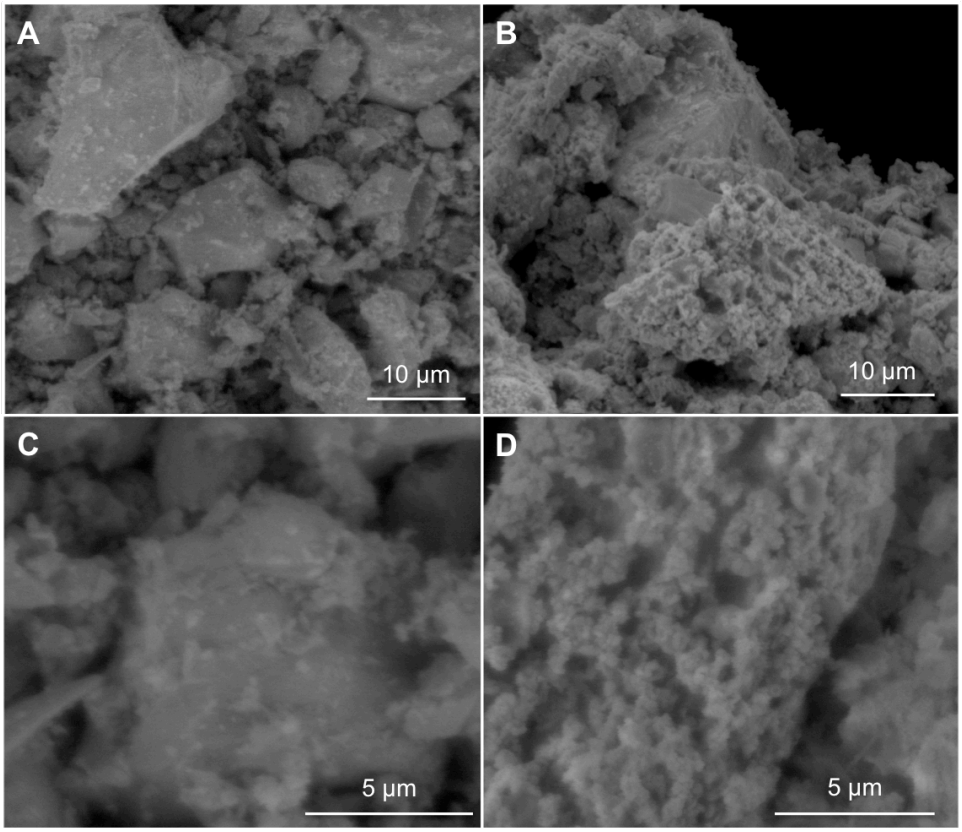

Figure 7. Secondary electron micrographs at variable pressure of cinnabar powder samples. Images A and C show control red particles, those that had been exposed to neither saline solution nor light, which exhibit the characteristic rhombohedral/tabular habit of cinnabar. Images B and D show blackened cinnabar particles, those exposed to 0.1M NaCl solution and exposed to light over 21 days, exhibiting a more granular morphology.

4.4 Chemical change

EDS spot analysis and elemental mapping of cross-sections showed the presence of Na, Cl, Hg and S within both the altered and unaltered areas. Despite extensive investigations, no correlation could be made between the presence of chlorine and the color of the particle. Chlorine was present both in the red and black particles and was always found in association with sodium (Figure 8). The elemental concentrations and distribution (Figure 8C) suggested the presence of a sodium chloride phase rather than a mercury chloride-containing compound. However, a qualitative reduction of sulfur in the blackened particles was observed (Figure 8C – see map of S in the black particle). Standardless EDS spot analysis on the red and black particles in the powder samples confirmed lower sulfur to mercury ratio in

the black particles (Figure 9 and Table 4) and an enrichment in chlorine. The ratio of sulfur to mercury in the unadulterated particles is close to 1 whereas the altered areas show an average ratio of 0.9. This indicates a depletion of sulfur in the blackened particles.

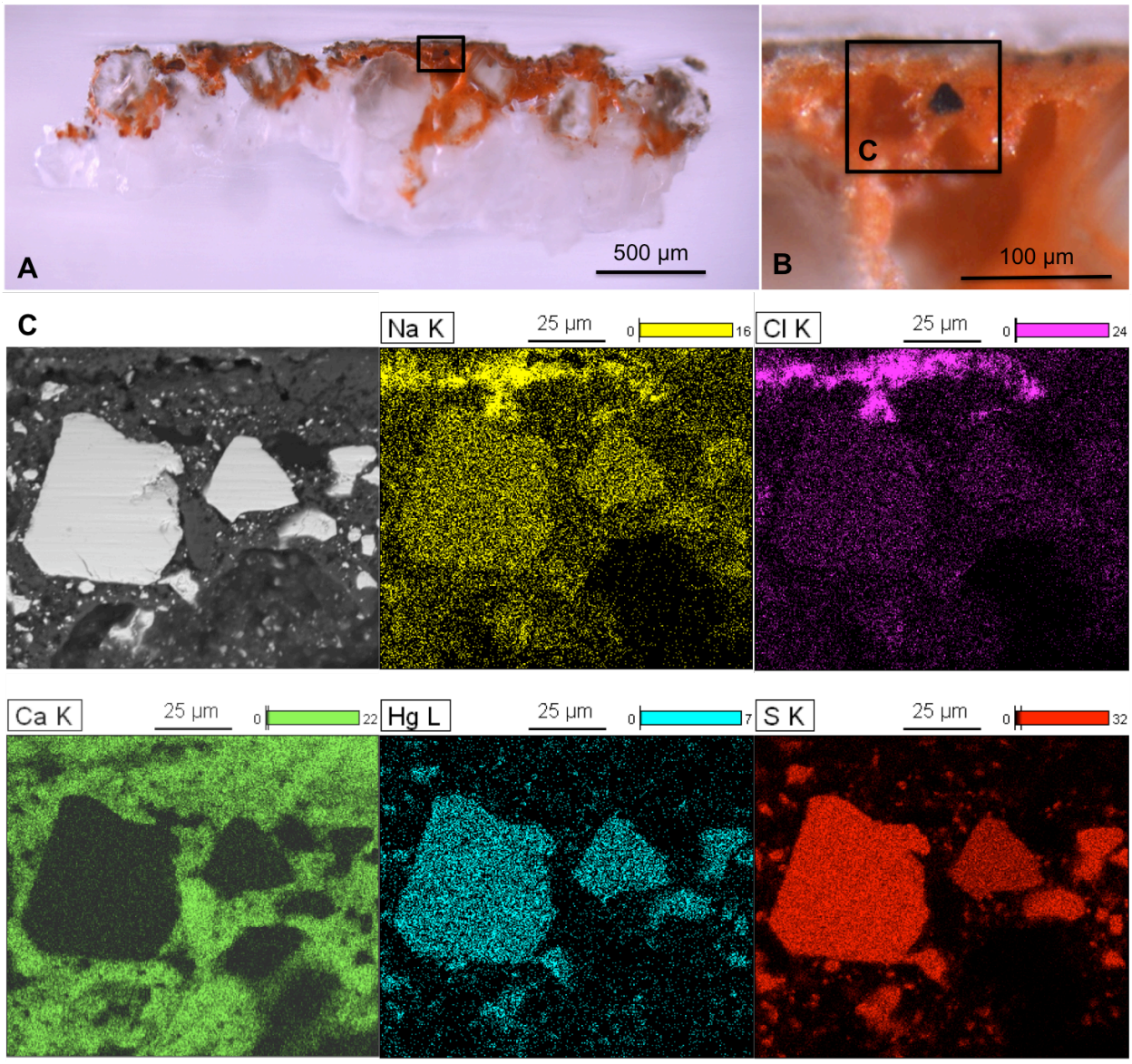

Figure 8. (A) Cross section removed from blacked section of a fresco block impregnated 0.1M NaCl solution, dried in the dark and subsequently exposed to light for 70 days. (B) Detail of the black and red particles in A. (C) SEM-BSE image and elemental maps indicating the spatial distribution of sodium, chlorine, calcium, mercury and sulfur within the red and black particles pictured.

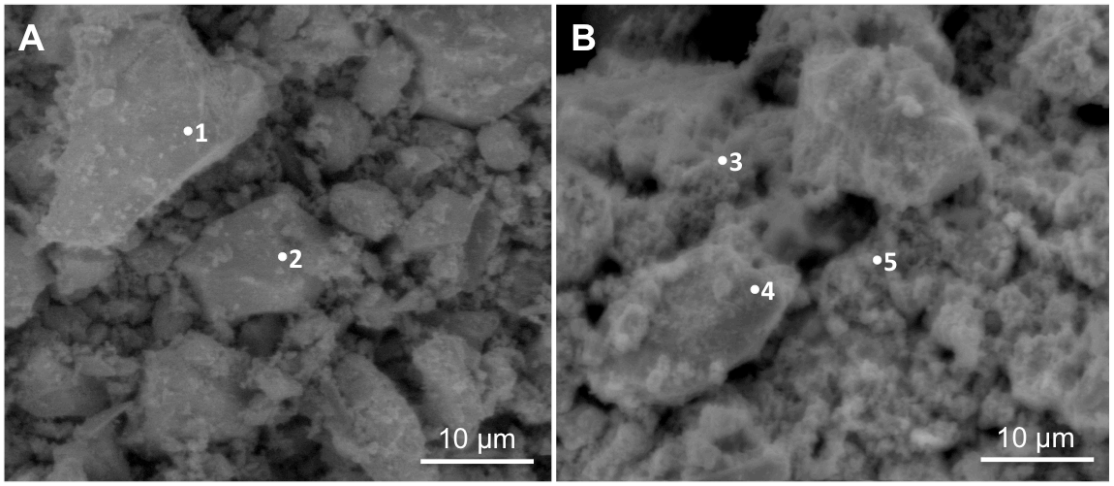

Figure 9. SEM images taken at 2000x magnification of bulk cinnabar particles; images were recorded with the secondary electron detector (SE) using the Low Vacuum Detector (LVD) and 7keV electron beam. Image A shows control red particles, those that had been exposed to neither saline solution nor light. Image B shows blackened cinnabar particles, those exposed to 0.1M NaCl solution and exposed to light over 21 days. Points 1-5 indicate areas analyzed using EDS (table 4).

Table 4. Standardless atomic % of elements measured on red unchanged (1 and 2) and black/altered (3, 4 and 5) cinnabar powder particles. EDS analysis was carried out at 20keV beam energy

Spot	O-Kα	Na-Kα	S-Kα	Cl-Kα	Hg-Lα
1	-	-	52.16 ±2.20	-	47.84 ±2.24
2	-	-	49.87 ±3.02	-	50.13 ±2.77
3	9.92 ±0.96	-	37.23 ±1.36	1.15 ±0.16	51.71 ±1.39
4	12.06 ±1.01	1.13 ±0.18	40.18 ±0.71	1.60 ±0.14	44.50 ±1.15
5	17.64 ±1.04	5.89 ±0.34	32.18 ±1.27	3.68 ±0.32	40.61 ±1.11

SEM-EDS analysis of a sample taken from the surface of the fresco before the infusion of 0.1M NaCl solution or exposure to light, showed a veil of cubic calcium carbonate crystals across the surface of the block characteristic of the carbonation process of calcium hydroxide (Figure 10A). Analysis of an area of blackened surface, after the introduction of the saline solution and light exposure, indicates a change in the appearance and elemental composition. The altered areas show the precipitation of thin, amorphous films of ~10 to 15 μm in diameter (Figure 10B) partially covering the calcium carbonate crystals. EDS spot analysis of the altered areas (Figure 10D) indicates a heightened presence of sulfur on the blackened surface. The presence of calcium, oxygen and carbon were detected on both altered and unaltered sample (Figure 10C and D), but sulfur was found to be present on the altered surfaces within the "amorphous islands."

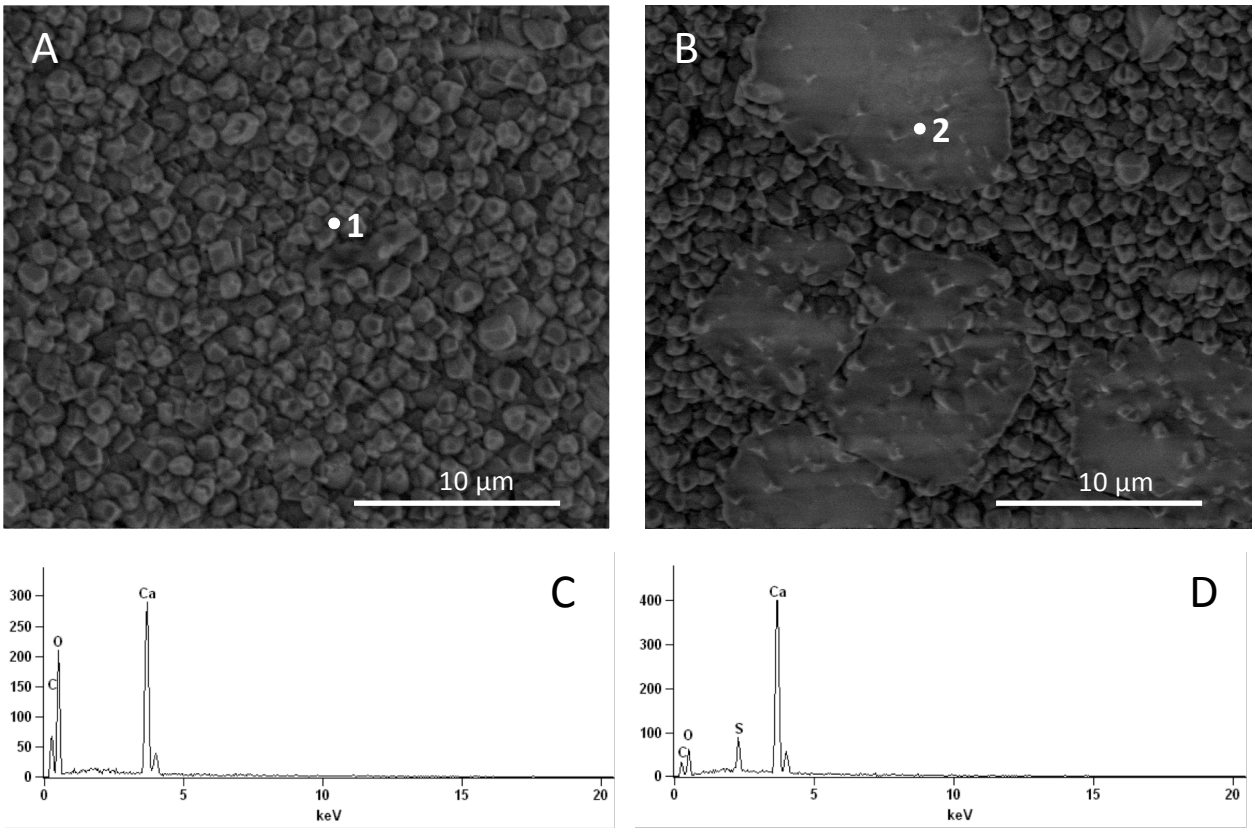

Figure 10. Secondary electron (SE) micrographs (A, B) and EDS spectra (C, D) of control and blackened cinnabar particles. A: SE micrograph of the surface of the simulated wall painting block showing the calcium carbonate particles resulting from the carbonation of the calcium hydroxide binder in the plaster. B: SE micrograph of the blackened fresco showing amorphous films of 10 to 15 µm diameter over the calcium carbonate crystals. Sample in image D was infused with 0.1M NaCl solution, dried in the dark and subsequently exposed to light for 70 days. C and D show EDS spectra taken from point 1 (Image A) and point 2 (Image B) from the control and blackened areas respectively.

4.5 Compound identification

XRD analysis of all samples recovered from the fresco blocks infused with NaCl showed consistent results. Cinnabar, calcite and halite were identified in all samples, and calomel was detected in most (Table 5; Figure 11; Figure 12; **Error! Reference source not found.**). The formation of calomel appears to be independent of: 1) exposure to light and 2) color of the sample. When blocks were dried in the dark and subsequently exposed to light, calomel was detected both before and after light exposure. Calomel was present in visually unaltered, as well as altered, areas of the block; it was detected on both red and

black areas of the samples suggesting that it is not directly responsible for the observed color change of the samples.

Table 5. Compounds identified on blocks in red and black areas both before and after light exposure

NaCl Solution (M)	Exposed to Light	Sample Color	Compounds Detected			
			α-HgS	$CaCO_3$	NaCl	Hg_2Cl_2
0.1M	Yes	Red	✓	✓	✓	✓
0.1M	Yes	Black	✓	✓	✓	✓
0.1M	No	Red	✓	✓	✓	✓
0.1M	Yes	Black	✓	✓	✓	✓
0.1M	Yes	Red	✓	✓	✓	✓
5M	No	Red	✓	✓	✓	✓
5M	Yes	Black	✓	✓	✓	–

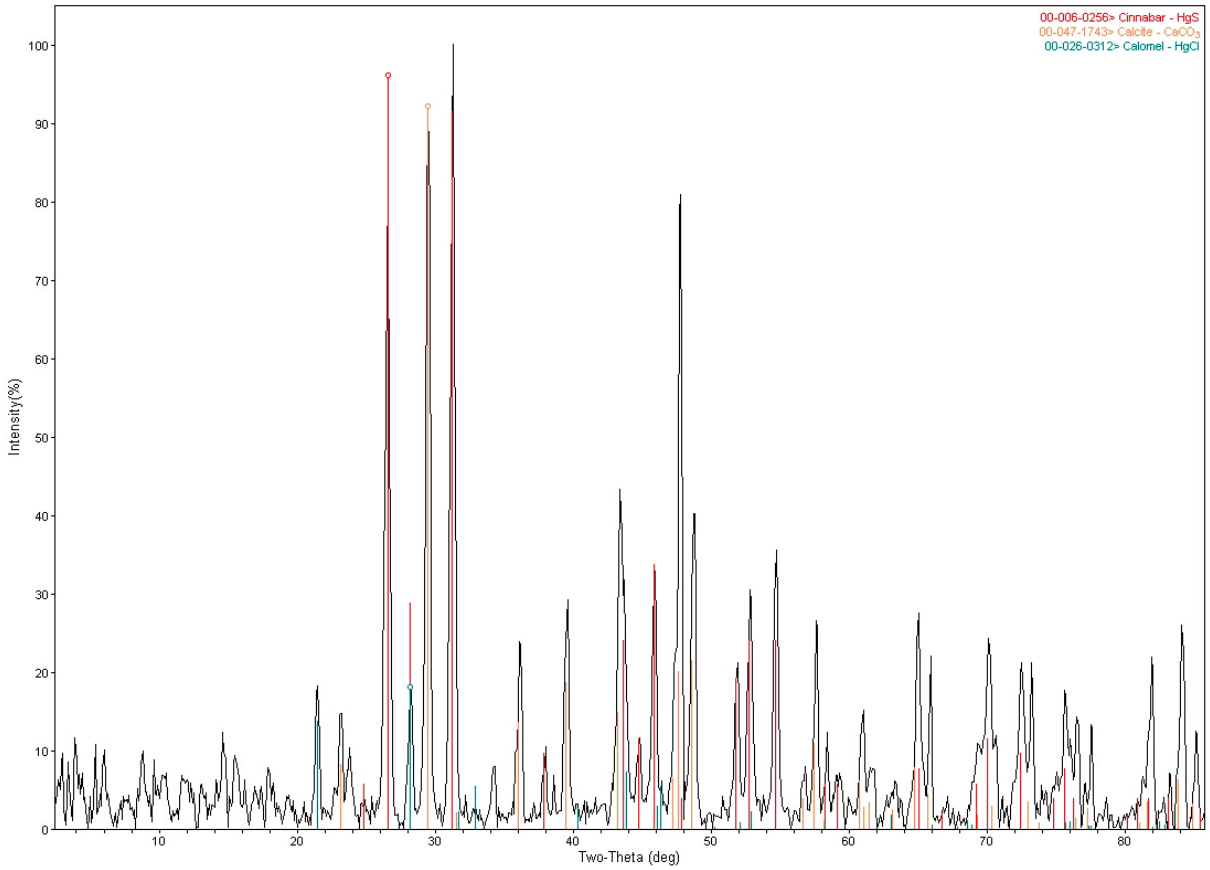

Figure 11. XRD diffractogram of a **red** area sampled from a block infused with 0.1 M NaCl solution, dried in dark and then exposed to light. The diffractogram shows the major phases identified that include cinnabar, calcite and calomel.

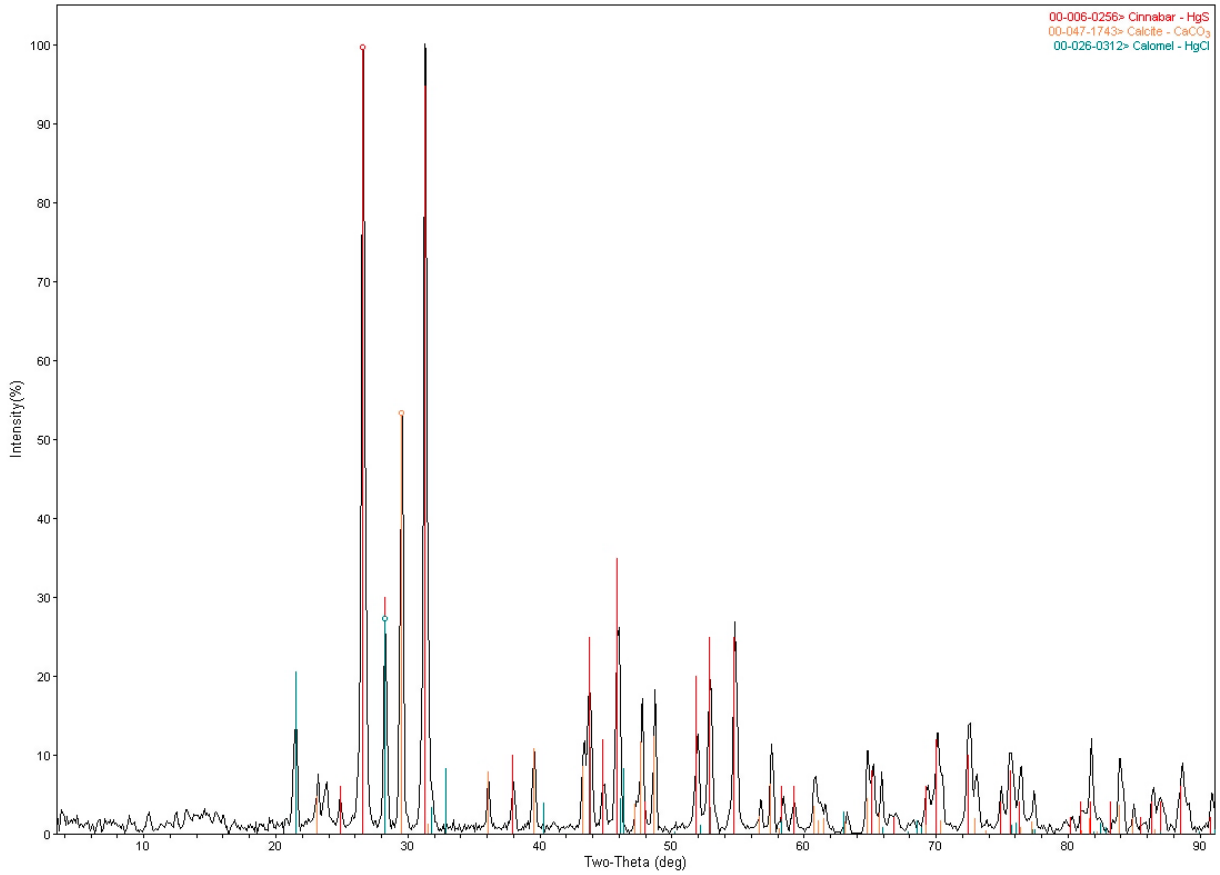

Figure 12. XRD diffractogram of a **black** area sampled from a block infused with 0.1M NaCl solution, dried in dark and exposed to light. The diffractogram shows the major phases identified that include cinnabar, calcite and calomel.

4.6 Desalination

Attempts to inhibit or retard the alteration process through desalination using successive compresses of deionized water (DI H_2O) water were unsuccessful. The surfaces of blocks desalinated, exhibited equal or enhanced discoloration when compared to those placed directly into the light (Figure 13).

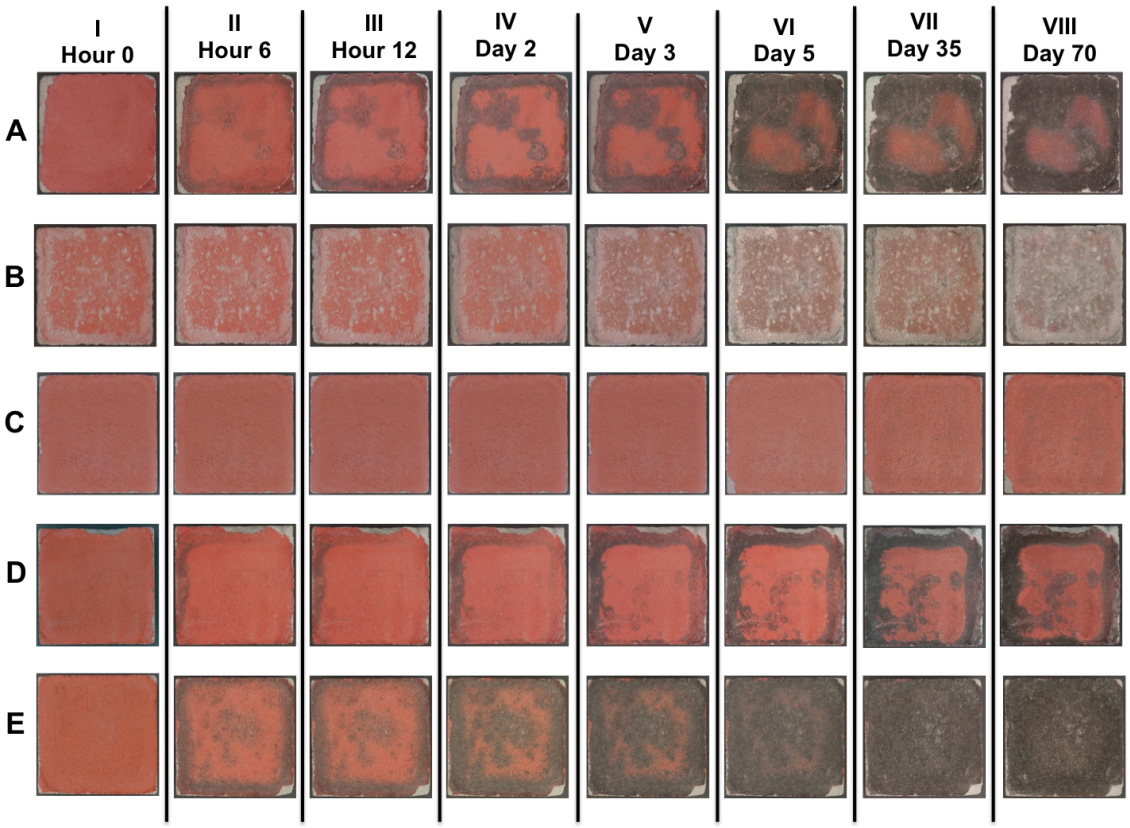

Figure 13. Images of fresco blocks during the 70 day period of light exposure in a windowsill at the Getty Villa in Malibu, CA. **A[1-VIII]:** Exposed to 0.1M NaCl solution, dried in dark prior to light exposure**; B[1-VIII]:** Exposed to 5M NaCl solution, dried in dark prior to light exposure; **C[1-VIII]:** Exposed to 0.1M NaCl solution; **D[1-VIII]:** Exposed to 0.1M NaCl solution, allowed to partially dry, poulticed and finally exposed to light; **E[1-VIII]:** Exposed to 5M NaCl solution, allowed to partially dry, poulticed and finally exposed to light.

CHAPTER 5: Thermodynamic Modeling

Thermodynamic calculations were carried out at 25°C and 1 bar using GEMS-PSI: Gibbs Energy Minimization Software package, version 2.0 (Kulik *et al*. 2003). GEMS is a broad-purpose geochemical modeling code which uses Gibbs energy minimization criterion and, in conjunction with information of the thermodynamic properties of phases (i.e., solids, liquid and air), computes equilibrium phase assemblage and speciation in a complex chemical system from its total bulk elemental composition. Chemical interactions involving distinct solid phases, solid solutions and the aqueous electrolyte(s) are considered simultaneously. Thermodynamic properties of solid and aqueous species were sourced from the GEMS-PSI standard database for minerals, and amended with additional information relevant to mercury containing phases. Input data for mercury-bearing solids were taken from (Radepont 2013) (Table 6).

Table 6. Free energies of formation of mercury-bearing phases considered in this study.

Phase	ΔG^0_f [kJ/mol]
Cinnabar (α-HgS)	-45.77
Metacinnabar (β-HgS)	-43.66
Calomel (Hg_2Cl_2)	-210.37
Mercuric Chloride ($HgCl_2$)	-180.30
Corderoite (α-$Hg_3S_2Cl_2$)	-406.99
Metallic Mercury; Quicksilver (Hg(0))	0

Thermodynamic modeling was carried out to provide insight into pure cinnabar alteration in the presence of sodium chloride, as well as when applied in the fresco technique. This is a generic equilibrium-based approach that does not take into consideration the impact of kinetic reactions or light that may significantly alter the phase assemblage found under real environmental conditions. However, it does serve as a useful guide for predicting phases, which are anticipated to be thermodynamically stable under particular conditions. Three possible scenarios were examined: (1) the bulk cinnabar pigment mineral; (2) pigment on a fully carbonated fresco surface and (3) pigment on carbonated fresco

surface which also contains a slight amount of $Ca(OH)_2$. Each of these systems was set to a 0.1M NaCl solution and modeled as a function of increasing amount of the atmospheric air, which was progressively added to the system (Figure 14; Figure 15; Figure 16).[7] Information regarding variations in the red-ox potentials (Eh) as well as pH of the aqueous solutions was recorded in order to assess their impact on phase formation.

5.1 Thermodynamic modeling predictions

The formation of cinnabar (α-HgS), corderoite (α-$Hg_3S_2Cl_2$), calomel (Hg_2Cl_2) and metallic mercury (Hg(0)) was predicted in all three scenarios. It was noticed that presence of calcium carbonate (Figure 15) or calcium hydroxide (Figure 16) significantly affected predicted phase assemblages when compared to the pure cinnabar pigment (Figure 14). The amount of atmospheric air, which was put in contact with the input compositions, has also greatly influenced redox potentials and pH of the simulated systems. Changes in the solid phases, which are predicted to precipitate, were directly linked to changes in the aqueous phase such as pH or the variations of the red-ox potential of the system. Despite its inclusion in the model and detection in cultural heritage materials, mercuric chloride ($HgCl_2$) was never predicted to precipitate for the conditions computed in this study. Metacinnabar (β-HgS) was also not anticipated to form under any of the scenarios simulated in this work (25°C and 1 bar pressure). The occurrence of corderoite (α-$Hg_3S_2Cl_2$) appears largely unaffected by the red/ox potential of the environment but was significantly impacted by changes in the pH; it only occurred when the pH of the aqueous solution was below 8. As a result, the formation of corderoite was significantly limited in the presence of calcium hydroxide ($Ca(OH)_2$) which presence elevated the pH of the system. Formation of metallic mercury (Hg(0)) was favored under reducing conditions and in a wide pH ranges. However, elevated pH, e.g. by

[7] It should be noted that a second 5M scenario was not simulated as current aqueous ion activity model implemented in GEMS can handle molar strengths only up to 2-3M.

the presence of calcium hydroxide ($Ca(OH)_2$), seemed to significantly favor formation of metallic mercury even under oxidizing conditions (Figure 16). The precipitation of calomel appears to require oxidizing conditions (Figure 14 Figure 15; Figure 16). As the amount of air which is put in contact with the material increases, the activity of $O_2(g)$ will be elevated. The redox potential will therefore increase, thus favoring the formation of calomel (Hg_2Cl_2) instead of corderoite (α-$Hg_3S_2Cl_2$). This observation is in agreement with findings reported in the literature (Radepont 2013). It was additionally observed that for certain oxidizing conditions when the pH is above 8 (Figure 15; Figure 16) gypsum ($CaSO_4 \cdot 2H_2O$) could be formed. This finding suggests that under certain circumstances gypsum may form in a cinnabar system without the 'necessity' of SO_2 species being supplied from an outdoor environment. Modeled scenarios indicate that transformation process of the cinnabar pigment is not straight forward and can be highly dependent on the nature of the system such as e.g. amount of air in contact (and resulting redox potential), pH or presence of accompanying phases such as $CaCO_3$, $Ca(OH)_2$.

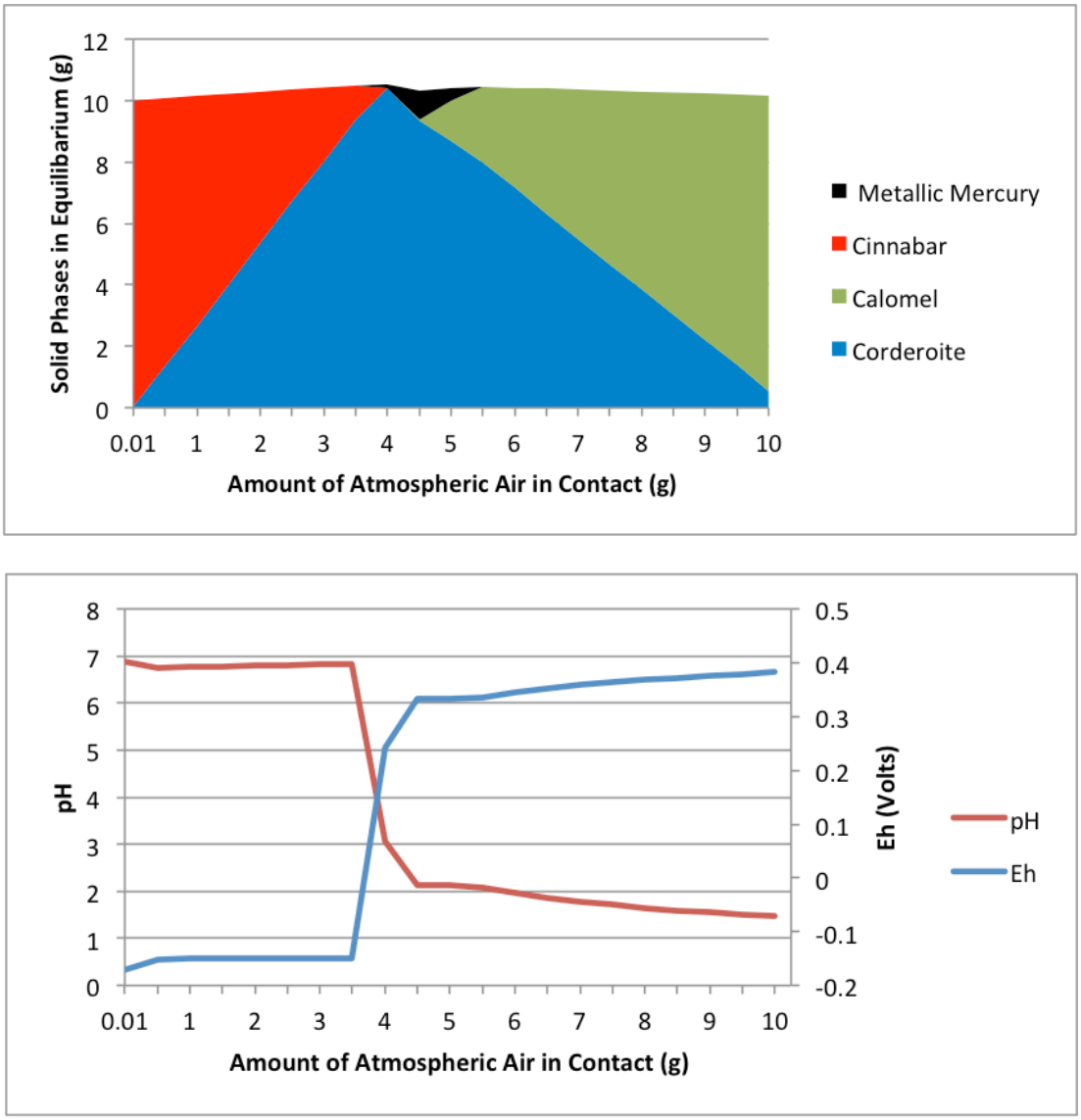

Figure 14. Top: Model showing changes in phase assemblage as a function of the amount of air being in contact with HgS mineral exposed to a 0.1M NaCl solution; equilibration of HgS (10 g) with H_2O (1000 g) and NaCl (5.844g) and various amounts of air (g). Bottom: Variation in pH aqueous phase and redox potential as a factor of amount of atmospheric air within the model.

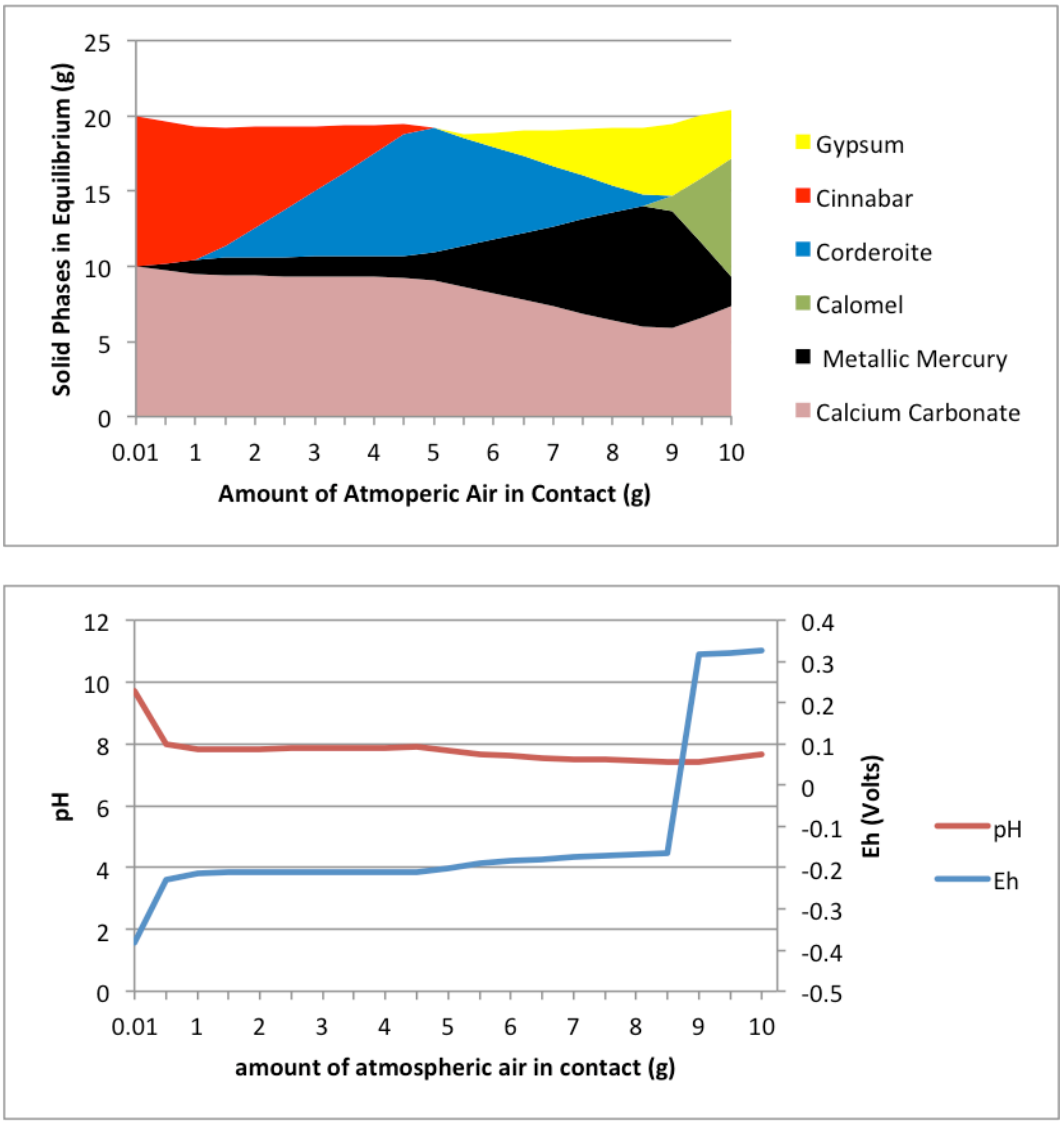

Figure 15. Top: Model showing changes in phase assemblage as a function of the amount of air being in contact with cinnabar pigment on fully carbonated fresco surface exposed to a 0.1M NaCl solution; equilibration of HgS (10 grams) and $CaCO_3$ (10 g) with H_2O (1000 g) and NaCl (5.844 g) and various amounts of air (g). Bottom: Variation in pH of aqueous phase and redox potential as a factor of amount of atmospheric air within the model.

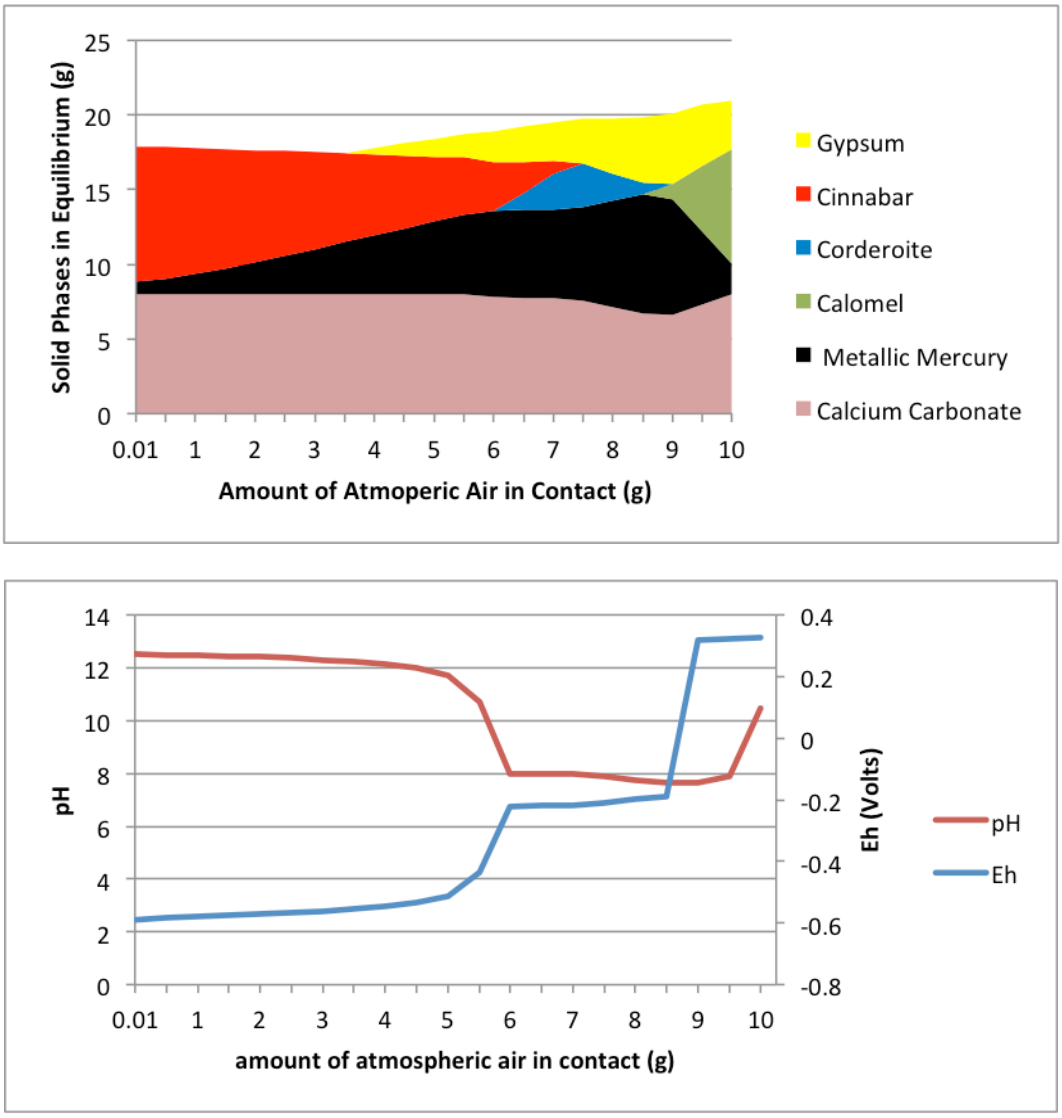

Figure 16. Top: Model showing changes in phase assemblage as a function of the amount of air being in contact with cinnabar pigment on recently constructed fresco surface – one that has not fully carbonated- which is exposed to a 0.1M NaCl solution; equilibration of HgS (10 grams) and 8g $CaCO_3$ and 2g of $Ca(OH)_2$ with H_2O (1000 g) and NaCl (5.844 g) and various amounts of air (g). It should be noted that at room temperature the solubility of $Ca(OH)_2$ is approximately 2g/L; therefore the compound is predicted to fully dissolve in this scenario and only alter the pH of aqueous phase. Bottom: Variation in pH of aqueous phase and redox potential as a factor of amount of atmospheric air within the model.

CHAPTER 6: Discussion

6.1 Conditions inducing the alteration

The work presented here confirms previous hypotheses that light and chlorine are the dominant factors in the darkening of cinnabar. This study has further indicated that high relative humidity also plays an essential role in the transformation processes. Exposure to Cl^-, light and humidity were required to induce significant alteration in the HgS pigmented fresco blocks and powder pigments.

Minor alterations were observed on the control samples exposed light. This is likely the result of trace amounts chlorine within the $Ca(OH)_2$ used to fabricate the test blocks. XRF analysis of the surface of the blocks prior to accelerated artificial weathering using saline solutions found an average of 0.03 Cl wt.% in each. While this amount is just below the 0.05 Cl wt% threshold known to induce the alteration (McCormack 2000), it appears adequate to provoke localized subtle darkening of the surface. The attribution of this darkening to chlorine in concert with light, rather than light alone, is supported by the results of laboratory trials involving powder cinnabar. Pure cinnabar powder exposed only to deionized water and placed into the sun under ambient conditions showed no evidence of blackening after 21 days of light exposure, while significant changes were observed in pigment powders exposed to 0.1M and 5M sodium chloride solutions.

The progression of the blackening of the fresco blocks from the outer edges inward can likely be linked to heightened chloride content of those areas. During drying, highly concentrated NaCl solution formed along the sides. Air circulation at the rougher, more porous edges allowed for enhanced evaporation over the smoothed, pigmented surface creating localized areas with high concentration of chlorine ions. Upon drying, the thickest halite crusts were found along the sides of each block. Interestingly, the correlation between increased Cl^- concentration and enhanced blackening was noted when comparing alteration on pigment powder samples treated with 0.1 and 5M NaCl solution, but not

in the blocks. While pigment powders treated with 5M NaCl solution, darkened more swiftly and pervasively then those treated with 0.1M NaCl, there was no discernable difference between the rate or degree of darkening of blocks treated with 5M NaCl and 0.1M NaCl. The lack of enhanced blackening on blocks treated with 5M solution, may be attributed to the layer of halite which had formed over the surface. The halite crystals could have acted as retardants to the rate of darkening in two ways: (1) by partially filtering/blocking the light and (2) by the hygroscopic nature of NaCl acting as a desiccant and absorbing moisture, which as shown in this study it is an essential factor for the alteration of cinnabar.

The identification of the specific wavelength(s) of electromagnetic radiation that favor/provoke this alteration was beyond the scope of this study. It is notable, however, that during experiments carried out by Radepont *et al.* (2011: 962) cinnabar pellets exposed to NaCl solutions under UV irradiation required >120 days for the surface to show color change as compared to 6 hours in the trials here. While differences in the experimental procedures prevent direct comparison, the disparity is dramatic and may indicate that visible as well as ultra violet wavelengths play an important role in the alteration process.

6.2 Alteration products and possible causes of darkening

6.2.1 Mercury-chloride containing Compounds

XRD analysis detected the presence of a single mercury-chloride compound. Calomel was identified on the surface of fresco samples exposed to saline solution, both before and after exposure to light. The formation of calomel in samples prior to light exposure is significant to understanding the possible causes of color alteration in cinnabar and stands in opposition to previous reaction mechanisms proposed to explain the pigment's color change. While thermodynamic modeling of an HgS, NaCl, H_2O containing system predicted the formation of calomel under certain conditions (Figure 14; Figure 15; Figure 16), the reaction mechanism previously proposed by scholars, largely suggests that calomel is

formed as part of a secondary or tertiary step, often after exposure to light. Keune and Boon (2005) proposed that chlorine serves to catalyze the photochemical redox of Hg(II)S into elemental Hg(0) and S(0). Subsequently, Cl^- and Hg(0) reacts to form $HgCl_2$ and HgS to form corderoite ($Hg_3S_2Cl_2$) and S(0). Upon exposure to light, the photosensitive corderoite, degrades into calomel (Hg_2Cl_2). This is followed by the light-induced disproportionation of calomel into Hg(0) and mercury(II) chloride ($HgCl_2$) (Equation 2).

$$Hg_2Cl_2 \rightarrow HgCl_2 + Hg$$

Equation 2. Disproportionation reaction of calomel.

Spring and Grout (2002) also supports that in the presence of light corderoite degrades to form calomel as well as sulfur and metacinnabar (β-HgS).

$$\alpha\text{-}Hg_3S_2Cl_2 \rightarrow Hg_2Cl_2 + S + \beta\text{-}HgS$$

Equation 3. Degradation of corderoite to form calomel, sulfur and metacinnabar.

Radepont *et al.* (2011) on the other hand suggested that cinnabar (α-HgS) is transformed to calomel via mercury sulfo-chloride intermediates; however, unlike Keune and Boon (2005) or Spring and Grout (2002), they do not explicitly state that light it required for these reactions to occur.

$$\alpha\text{-}HgS \rightleftharpoons \gamma\text{-}Hg_3S_2Cl_2 \rightleftharpoons \alpha\text{-}Hg_3S_2Cl_2 \rightleftharpoons Hg_2Cl_2$$

Equation 4. Cinnabar transformation to calomel through intermediate sulfo-chloride intermediates.

These studies all describe corderoite as a phase preceding the formation of calomel during the alteration process. Indeed, thermodynamic modeling of an Hg, NaCl, H_2O containing system predicted the formation of corderoite (Figure 14; Figure 15; Figure 16), a mercury sulfo-chloride which has been detected by several other scholars on altered cultural heritage materials. In the experimental study however, corderoite has not been identified. Clearly this difference is significant, and the lack of

corderoite here requires additional investigations. Several possible explanations are, therefore, explored.

The pH of the saline solution for example during artificial weathering may explain the presence or absence of particular compounds and some phases are more stable. Parks and Nordstrom (1979) predicts that corderoite will occur only under acidic conditions, and thermodynamic modeling carried out in this study also supported these findings. Corderoite was only predicted to occur for the conditions where pH was below 8. The presence of small amounts of un-reacted $Ca(OH)_{2,}$ within the fresco blocks used in this experiment created an alkaline environment during the artificial weathering process. The pH of the saline solutions was tested before and after infusion, with a Merck pH strip. Indicator strips dipped into the solution when the blocks were first placed into contact with saline solution showed a pH of 7, after 12 hours in contact the solution had a pH of 12. This suggests that the unreacted $Ca(OH)_2$ present within the block came into equilibrium with the saline solution. However, experiments carried out by Radepont (2013), in which NaOCl with pH 12 was used as the chlorine source, formed corderoite; thus, indicating that an acidic environment, as predicted in some thermodynamic models, is not the determining factor for its formation. Therefore, the lack of detection may be attributed to the timing of measurement after exposure to light. Radepont (2013) found that neither corderoite nor calomel was consistently detectable by XRD over time, within a single weathered sample. It is possible, therefore, that the formation of corderoite and calomel are time sensitive. Corderoite could have been present for some period on the fresco blocks, but have gone undetected.

The presence of calomel both before and after light-induced blackening, as well as the inability to detect corderoite, indicates that color-shift observed during alteration cannot be attributed to the presence of either mercury-chloride compounds.

6.3 Formation of metallic mercury

The photosensitivity of calomel is well documented. In the presence of light, calomel undergoes a disproportionation reaction (Barta *et al.* 1987) and degrades in black metallic mercury and in white mercury(II) chloride (Equation 2).

The formation of metallic mercury is predicted by thermodynamic modeling to occur within a HgS-NaCl-H_2O-containing system. Attempts to visually observe metallic mercury on the surface of degraded particles using SEM were unsuccessful. Nor was there evidence of the "hot spots" which Keune and Boone (2005) have suggested indicated the presence of metallic mercury on blackened particles. It should also be noted that mercury(II) chloride was untraceable by XRD on altered surfaces either. However, it is possible that the amount of material formed was below the instrument's detection limit. The fact the blackening occurs at the time of light exposure and the amorphization of the blackened particles suggests nano-particle of metallic mercury are responsible for the color shift from red to back.

6.4 Calcium-sulfur containing compounds

SEM analysis indicates the possible formation of a calcium-sulfur phase on the surface. The specific compound was not identified by XRD. However, the phase observed during SEM analysis is likely the very early stages of the formation of gypsum ($CaSO_4 \cdot 2H_2O$) at the fresco surface. This is a phenomenon predicted by thermodynamic modeling and previously observed in altered cinnabar on fresco samples recovered from Pompeii (Cotte *et al*. 2006, Radepont *et al.* 2011 and Radepont 2013) and from the Santa Maria Church in Northern Spain (Perez-Alonso 2006). As proposed by Cotte *et al.* (2006) it appears that sulfur lost by the cinnabar particles during the alteration process reacts with oxygen present in the environment.

$$S + O_2 \rightarrow SO_2$$

Equation 5. Oxidation of sulfur by the atmosphere.

This SO_2 subsequently reacts with the $Ca(OH)_2/CaCO_3$ (fresco binder) at the surface to form gypsum (Equation 6).

$$SO_2 + CaCO_3 + ½O_2 + 2H_2O \rightarrow CaSO_4 \cdot 2H_2O + CO_2$$

Equation 6. Reaction of SO_2 with the $CaCO_3$ substrate to form gypsum.

It is possible that external sources of SO_2, e.g. combustion product present in the environment, have in some cases played a role in the formation of gypsum on cinnabar pigmented historic wall paintings or archaeological frescoes unearthed for extended periods, as has been documented on other calcareous cultural heritage materials (Gauri *et al.* 1999, Ausset *et al*. 1992, Charcola and Ware 2002, Charola *et a*l. 2007, Toniolo *et al.* 2009). However, the formation of calcium-sulfur compounds, under controlled conditions and in such a short timespan, would suggests that the formation of gypsum is a byproduct of the alteration process on calcium-based substrates and does not necessarily require an additional SO_2 source from an outside environment. Though not the primary source of blackening, the presence of fine dust particles trapped within the gypsum layer during formation, likely exacerbates the darkening of cinnabar pigmented calcium-based substrate of materials housed in an outdoor setting.

6.5 Assessment of desalination and alternate drying methodology as blackening inhibitor

Efforts to inhibit or limit alteration through the implementation of alternate drying methodologies (drying in the dark to limit moisture at the time of light exposure) or the use of desalination procedures proved ineffectual. In fact, the treatments employed lead to increased rather then reduced darkening. It appears that these conservation treatments, which prolonged the period of contact with NaCl solution with the cinnabar, create an environment conducive to the formation of calomel.

Drying the blocks in the dark slowed significantly the rate at which moisture was lost. It took 14 days for those placed into the dark to come to a static weight, while those placed directly into the sun were dry after 3 days. This extended drying time allowed a high concentration solution to form at surface of the block and remain in contact with the surface for a prolonged period as it dried. Repeated desalination attempts of the blocks with DI H_2O to remove the salts similarly resulted in prolonged contact of NaCl solutions; attempts to reduced salts required multiple sequences of poulticing leaving block exposed for ~15 days. The solubility of calomel, while significantly higher than cinnabar, is quite low (0.2 mg/100 mL). Consequently, once the compound is formed only a small portion may be dissolved and absorbed into the cellulosic fibers during the poulticing process though diffusion and advection processes. In the case of the trials carried out here, the rate of calomel formation appeared to surpass the rate at which was removed.

Allowing the blocks to dry prior to placing them into the light failed to limit darkening. However, drying chlorine-contaminated cinnabar quickly and keeping the material under desiccating conditions appears to reduce and slow down blackening. Moreover, increasing the relative humidity (RH) of the environment in which the cinnabar is housed dramatically accelerates the blackening. Cinnabar pigment treated with 0.1M NaCl solution and stored at <5% RH showed no discernable darkening when placed into the light for 21 days. While pigment treated in the same manner and stored at ~70% RH showed significant blackening. The rate of reaction appears significantly reduced in the absence of moisture. It is possible that water is acting a medium to carry ions necessary for the reaction to occur.

CHAPTER 7: Conclusions and Conservation Recommendations

The experimental and theoretical research conducted here, supports pervious assertions that chlorine and light play pivotal roles in the blackening process of cinnabar. In the absence of either, the color change from red to black will not occur. However, the specific mechanism by which this transformation occurs is still not clearly understood. Significantly, in contrast to pervious studies, the research conducted here indicates that the processes and intermediate phases responsible for the chemical alteration of the cinnabar begin prior to light exposure. Calomel may occur in the absence of light. Therefore, while steps may be taken to limit the blackening of the surface, complete inhibition of the alteration process through drying of the fresco prior to light exposure or the removal of chlorine ions through poulticing have proven ineffectual.

Recommendations for conservators charged with the preservation of cinnabar pigmented frescos are, therefore, limited. Tests for chlorides should be conducted at the time of excavation to determine the risk of blackening. A variety of possible detection techniques are available including: chloride test strips, colorimetric indicator kits and microchemical tests, as well as instrumental analysis including chloride ion selective electrode, ion chromatography, XRD, Raman and XRF. However, care must be taken to ensure that the testing methodology employed is adequately sensitive. Cinnabar pigmented surfaces with > 0.01 Cl wt.% content should be considered as risk for alteration. Those conserving wall paintings after excavation must, additionally, note that industrial and natural sources, including chlorofluorocarbons and sea spray, present within the environment when in combination with elevated relative humidity could induce alteration at a later time.

As attempts to reduce the amount of Cl^- have proven ineffective at decreasing the risk of alteration, interventions should be focused on limiting light and moisture. Where chlorides are present excavation should be carried out in the shade of a tent and light-blocking materials placed in front

cinnabar-pigmented surfaces, which are not currently under active excavation. Fragments that are found ex-situ should be promptly removed from the ground and stored in a darkened environment. It may also be prudent to speed drying and subsequently house such dissociated materials with a desiccant to limit continued formation of Hg-Cl containing compounds. However, it is important to understand that such a procedure could cause surface and subsurface efflorescence of other soluble salts causing visual and mechanical damage to the artifact. For this reason, such a treatment should only be carried out with caution and when all other parameters and risks have been carefully evaluated.

Appendix 1

XRD results for samples removed from fresco blocks before and after exposure to saline solution and light.

Control: No NaCl, No H_2O, No Light

d-Spacing	Height	Height Percent	Area	Area Percent	Cinnabar	Calcite
31.0577	138	8.1	684	11.0		
11.5281	61	3.6	306	4.9		
9.8097	39	2.3	105	1.7		
9.0989	87	5.1	275	4.4		
6.6959	45	2.6	108	1.7		
6.0280	243	14.3	692	11.2		
5.6889	93	5.5	261	4.2		
4.5436	83	4.9	264	4.3		
4.1543	112	6.6	430	6.9		
3.8485	182	10.7	1060	17.1		3.85/1
3.7254	72	4.2	473	7.6		
3.3553	347	20.4	1410	22.7	3.36/X	
3.1655	131	7.7	595	9.6	3.17/3	
3.0221	1700	100.0	6199	100.0		3.04/X
2.8643	450	26.5	1797	29.0	2.86/X	
2.6164	97	5.7	237	3.8		
2.4880	170	10.0	648	10.4		2.49/1
2.2771	407	23.9	1467	23.7		2.28/2
2.0841	693	40.8	3116	50.3	2.07/3	2.09/2
1.9752	84	5.0	174	2.8	1.98/4	
1.9038	413	24.3	2207	35.6		1.91/2
1.8672	487	28.6	2092	33.7		1.88/2
					1.77/2	
1.7303	127	7.5	552	8.9	1.74/3	
1.6779	177	10.4	1016	16.4	1.68/3	
1.6187	133	7.9	573	9.2		1.60/1
1.5974	428	25.2	1519	24.5		
1.5185	364	21.4	1901	30.7		
1.4690	65	3.8	188	3.0		
1.4349	385	22.7	1783	28.8		
1.4168	166	9.8	693	11.2		
1.3520	118	7.0	732	11.8		
1.3342	158	9.3	599	9.7		
1.3032	109	6.4	1030	16.6		
1.2916	149	8.8	1744	28.1		
1.2545	94	5.5	1010	16.3		
1.2434	126	7.4	537	8.7		
1.2312	170	10.0	691	11.2		
1.2226	33	2.0	88	1.4		
1.1752	402	23.6	1687	27.2		
1.1498	467	27.5	1690	27.3		
1.1386	195	11.5	709	11.4		
1.1243	148	8.7	730	11.8		
1.1187	78	4.6	604	9.7		
1.1029	81	4.8	248	4.0		

MN_19_0.1M, dried in dark and exposed to light, red area

d-Spacing	Height	H%	Area	A%	Cinnabar	Calcite	Halite	Calomel
22.3457	135	9.0	560	9.2				
14.6828	130	8.6	422	7.0				
11.3487	42	2.8	188	3.1				
10.0303	128	8.5	589	9.7				
7.3871	54	3.6	293	4.8				
6.0404	142	9.4	428	7.1				
4.1351	232	15.4	604	10.0				4.15/8
						3.85/1		
3.8326	184	12.2	725	12.0				
3.7363	122	8.1	401	6.6				
3.3504	1185	78.5	4864	80.2	3.36/X	3.04/X		
							3.26/1	
3.1554	261	17.3	999	16.5	3.17/3			3.17/X
3.0251	1368	90.6	5123	84.5				
2.8565	1509	100.0	6064	100.0	2.86/X			
							2.82/x	2.82/1
								2.73/3
2.6164	94	6.2	260	4.3				
2.4839	341	22.6	1339	22.1		2.49/1		
2.3681	135	8.9	412	6.8				
2.2754	407	26.9	1540	25.4		2.28/2		
								2.24/1
2.0822	625	41.4	3845	63.4	2.07/3	2.09/2		2.07/4
2.0219	138	9.2	554	9.1			1.99/6	
1.9752	431	28.5	1457	24.0	1.98/4			1.97/2
								1.96/3
1.9027	1182	78.3	4248	70.1		1.91/2		
1.8670	599	39.7	2851	47.0		1.88/2		
1.7606	280	18.6	1064	17.5	1.77/2			
1.7316	423	28.0	1817	30.0	1.74/3			
1.6763	517	34.2	2133	35.2	1.68/3			
1.6201	93	6.1	274	4.5			1.63/2	
1.5982	323	21.4	838	13.8		1.60/1		
1.5579	52	3.5	114	1.9				
1.5184	168	11.1	738	12.2				
1.5053	60	4.0	175	2.9				
1.4680	63	4.2	376	6.2				
1.4335	390	25.9	1811	29.9				
1.4167	313	20.7	769	12.7			1.41/1	
1.3939	39	2.6	75	1.2				
1.3543	146	9.7	953	15.7				
1.3410	352	23.3	3080	50.8				
1.3026	305	20.2	2138	35.3				
1.2918	304	20.1	1155	19.1				
1.2561	213	14.1	1262	20.8			1.26/1	
1.2441	141	9.3	351	5.8				
1.1751	295	19.6	1427	23.5				
1.1497	329	21.8	901	14.9			1.15/1	

MN_19_0.1M, dried in dark and exposed to light, blackened area

d(≈)	Height	H%	Area	A%	Cinnabar	Calcite	Halite	Calomel
9.9008	108	1.9	377	1.8				
8.5002	129	2.3	421	2.0				
6.6585	95	1.7	286	1.4				
4.1321	724	13.0	2393	11.4				4.15/8
3.8331	360	6.5	1440	6.9		3.85/1		
3.7281	309	5.6	1475	7.1				
3.5748	226	4.1	572	2.7				
3.3419	5517	99.3	20905	100.0	3.36/X			
							3.26/1	
3.1508	1457	26.2	4014	19.2	3.17/3			3.17/X
						3.04/X		
3.0198	2944	53.0	8730	41.8				
2.8539	5559	100.0	20505	98.1	2.86/X		2.82/X	2.82/1
								2.73/3
2.4854	354	6.4	940	4.5		2.49/1		
2.3659	295	5.3	620	3.0				
2.2757	530	9.5	1499	7.2		2.28/2		
								2.24/1
2.0664	1022	18.4	4855	23.2	2.07/3			2.07/4
						2.09/2		
2.0191	298	5.4	1175	5.6				
1.9730	1433	25.8	6217	29.7	1.98/4		1.99/6	1.97/2
								1.96/3
1.9029	925	16.6	3525	16.9		1.91/2		
1.8681	997	17.9	2905	13.9		1.88/2		
					1.77/2			
1.7584	655	11.8	2713	13.0	1.74/3			
1.7294	1032	18.6	4224	20.2				
1.6740	1451	26.1	5373	25.7	1.68/3			
1.6215	198	3.6	560	2.7		1.60/1	1.63/2	
1.5577	185	3.3	649	3.1				
1.5202	375	6.7	2117	10.1				
1.5049	186	3.3	1121	5.4				
1.4360	560	10.1	2012	9.6				
1.4165	406	7.3	1319	6.3			1.41/1	
1.3960	102	1.8	668	3.2				
1.3728	58	1.1	162	0.8				
1.3533	275	4.9	1119	5.4				
1.3401	665	12.0	4385	21.0				
1.3017	744	13.4	3945	18.9				
1.2657	279	5.0	1001	4.8			1.26/1	
1.2556	520	9.3	3014	14.4				
1.2449	422	7.6	1861	8.9				
1.2318	259	4.7	878	4.2				
1.1944	76	1.4	223	1.1				
1.1768	629	11.3	2928	14.0				
1.1520	493	8.9	2158	10.3			1.15/1	
1.1401	169	3.0	370	1.8				
1.1245	260	4.7	879	4.2				
1.1191	191	3.4	907	4.3				
1.1021	461	8.3	2596	12.4				

MN_19_0.1M, dried in dark/ no light exposure, red area

d(≈)	Height	H%	Area	A%	Cinnabar	Calcite	Halite	Calomel
13.8763	85	2.1	562	3.7				
12.4944	67	1.6	424	2.8				
8.8774	34	0.8	66	0.4				
6.7141	116	2.8	496	3.2				
6.0517	85	2.1	214	1.4				
4.8823	144	3.5	524	3.4				
4.1366	796	19.4	2740	17.9				4.15/8
3.8390	329	8.0	1486	9.7		3.85/1		
3.7378	228	5.5	866	5.7				
3.3520	1383	33.6	7739	50.5	3.36/X			
							3.26/1	
3.1567	375	9.1	1238	8.1	3.17/3			3.17/X
3.0268	4114	100.0	15319	100.0		3.04/X		
2.8575	2055	50.0	8371	54.6	2.86/X			
							2.82/X	2.82/1
								2.73/3
2.6177	379	9.2	1418	9.3				
2.4889	663	16.1	3007	19.6		2.49/1		
2.3646	105	2.6	225	1.5				
2.2805	1066	25.9	3731	24.4		2.28/2		
								2.24/1
2.0889	1093	26.6	7131	46.6	2.07/3	2.09/2		2.07/4
2.0189	229	5.6	1307	8.5				
1.9764	687	16.7	3843	25.1	1.98/4		1.99/6	1.97/2
								1.96/3
1.9066	1278	31.1	6881	44.9		1.91/2		
1.8704	1375	33.4	6048	39.5		1.88/2		
1.7899	123	3.0	460	3.0				
1.7610	330	8.0	1728	11.3	1.77/2			
1.7327	425	10.3	2345	15.3	1.74/3			
1.6772	632	15.4	3025	19.8	1.68/3			
1.6248	211	5.1	901	5.9			1.63/2	
1.6022	591	14.4	2548	16.6		1.60/1		
1.5804	195	4.7	893	5.8				
1.5595	71	1.7	623	4.1				
1.5222	380	9.2	2720	17.8				
1.5092	175	4.2	2083	13.6				
1.4702	144	3.5	825	5.4				
1.4396	456	11.1	2804	18.3				
1.4184	250	6.1	1012	6.6			1.41/1	
1.3549	170	4.1	824	5.4				
1.3399	302	7.3	2285	14.9				
1.2941	234	5.7	2629	17.2				
1.2560	184	4.5	1181	7.7			1.26/1	
1.2473	192	4.7	1219	8.0				
1.2334	156	3.8	721	4.7				
1.1771	283	6.9	1725	11.3				
1.1534	340	8.3	1515	9.9			1.15/1	
1.1422	223	5.4	714	4.7				

MN_14_0.1M, exposed to light, black area

d(≈)	Height	H%	Area	A%	Cinnabar	Calcite	Halite	Calomel
31.9154	179	4.9	708	5.7				
11.8471	67	1.9	392	3.2				
9.0335	76	2.1	297	2.4				
6.0349	178	4.9	556	4.5				
5.7402	86	2.4	259	2.1				
4.1733	395	10.9	1149	9.3				4.15/8
3.8667	418	11.5	1437	11.6		3.85/1		
3.6179	70	1.9	138	1.1				
3.3755	2578	70.9	9708	78.3	3.36/X			
							3.26/1	
3.1776	775	21.3	2189	17.6	3.17/3			3.17/X
3.0411	3635	100.0	12132	97.8		3.04/X		
2.8742	3152	86.7	12405	100.0	2.86/X			
							2.82/X	2.82/1
								2.73/3
2.5024	446	12.3	1395	11.2		2.49/1		
2.3838	238	6.6	736	5.9				
2.2914	814	22.4	2817	22.7		2.28/2		
2.2348	70	1.9	247	2.0				2.24/1
2.0798	1388	38.2	6344	51.1	2.07/3	2.09/2		2.07/4
2.0306	466	12.8	1138	9.2				
1.9863	867	23.8	4036	32.5	1.98/4		1.99/6	1.97/2
								1.96/3
1.9141	1673	46.0	6682	53.9		1.91/2		
1.8795	905	24.9	3057	24.6		1.88/2		
1.7703	539	14.8	2163	17.4	1.77/2			
1.7394	794	21.8	3517	28.4	1.74/3			
1.6838	1186	32.6	4581	36.9	1.68/3			
1.6301	164	4.5	623	5.0			1.63/2	
1.6080	462	12.7	1542	12.4		1.60/1		
1.5871	242	6.7	821	6.6				
1.5650	174	4.8	732	5.9				
1.5291	203	5.6	1337	10.8				
1.5126	102	2.8	1244	10.0				
1.4747	105	2.9	618	5.0				
1.4402	348	9.6	2478	20.0				
1.4230	449	12.4	1189	9.6				
1.4041	71	2.0	390	3.1			1.41/1	
1.3590	222	6.1	1080	8.7				
1.3456	430	11.8	2779	22.4				
1.3078	387	10.7	2467	19.9				
1.2718	159	4.4	643	5.2				
1.2614	377	10.4	2152	17.4			1.26/1	
1.2501	212	5.8	1053	8.5				
1.2356	168	4.6	1074	8.7				
1.1896	84	2.3	256	2.1				
1.1812	170	4.7	593	4.8				
1.1559	155	4.3	1186	9.6			1.15/1	
1.1284	94	2.6	297	2.4				
1.1217	128	3.5	486	3.9				
1.1079	76	2.1	274	2.2				
1.0829	108	3.0	250	2.0				

MN_14_0.1M, exposed to light, red area

d(≈)	Height	H%	Area	A%	Cinnabar	Calcite	Halite	Calomel
22.1086	129	4.7	565	4.8				
6.7521	72	2.6	143	1.2				
5.9895	60	2.2	126	1.1				
4.9104	175	6.4	802	6.8				
4.1408	245	9.0	779	6.6				4.15/8
3.8398	277	10.1	1326	11.3		3.85/1		
3.3544	2586	94.7	10869	92.4	3.36/X			
							3.26/1	
3.1628	627	23.0	2045	17.4	3.17/3			3.17/X
3.0294	2467	90.4	8984	76.4		3.04/X		
2.8636	2730	100.0	11760	100.0	2.86/X			
							2.82/X	2.82/1
								2.73/3
2.6214	274	10.0	782	6.7				
2.4830	1028	37.7	3982	33.9		2.49/1		
2.3699	167	6.1	549	4.7				
2.2759	1030	37.7	4360	37.1		2.28/2		
								2.24/1
2.0836	1286	47.1	6851	58.3	2.07/3	2.09/2		2.07/4
2.0243	158	5.8	454	3.9				
1.9775	717	26.3	2699	22.9	1.98/4		1.99/6	1.97/2
								1.96/3
1.9096	502	18.4	3336	28.4		1.91/2		
1.8722	604	22.1	3122	26.6		1.88/2		
1.7904	106	3.9	317	2.7				
1.7620	317	11.6	1199	10.2	1.77/2			
1.7327	726	26.6	3329	28.3	1.74/3			
1.6774	795	29.1	3593	30.6	1.68/3			
1.6197	286	10.5	1073	9.1			1.63/2	
1.5976	767	28.1	3459	29.4		1.60/1		
1.5604	132	4.8	480	4.1				
1.5190	397	14.5	1650	14.0				
1.4680	84	3.1	321	2.7				
1.4338	810	29.7	3547	30.2				
1.4180	104	3.8	283	2.4			1.41/1	
1.3568	125	4.6	408	3.5				
1.3431	271	9.9	2206	18.8				
1.3042	336	12.3	1839	15.6				
1.2681	104	3.8	338	2.9			1.26/1	
1.2568	265	9.7	1890	16.1				
1.2436	219	8.0	1203	10.2				
1.2341	87	3.2	273	2.3				
1.1955	56	2.1	281	2.4				
1.1790	199	7.3	1098	9.3				
1.1492	380	13.9	1494	12.7			1.15/1	
1.1383	145	5.3	462	3.9				
1.1254	117	4.3	691	5.9				
1.1197	51	1.9	177	1.5				
1.1041	150	5.5	668	5.7				

MN_3_5M, dried in dark, no light, red area

d(≈)	Height	H%	Area	A%	Cinnabar	Calcite	Halite	Calomel
10.1725	58	1.6	271	2.3				
9.1017	119	3.2	678	5.7				
6.0034	240	6.5	797	6.7				
5.6668	90	2.4	179	1.5				
5.2876	52	1.4	156	1.3				
4.1356	365	9.9	1256	10.5				4.15/8
3.8380	257	7.0	1421	11.9		3.85/1		
3.7389	153	4.1	908	7.6				
3.3443	2922	79.2	11094	92.7	3.36/X			
							3.26/1	
3.1501	833	22.6	2540	21.2	3.17/3			3.17/X
3.0243	3689	100.0	11252	94.0		3.04/X		
2.8527	3205	86.9	11970	100.0	2.86/X		2.82/X	2.82/1
								2.73/3
2.4877	267	7.2	845	7.1		2.49/1		
2.3676	168	4.6	530	4.4				
2.2770	477	12.9	1523	12.7		2.28/2		
								2.24/1
						2.09/2		
2.0677	566	15.3	2899	24.2	2.07/3			2.07/4
1.9797	755	20.5	3306	27.6	1.98/4		1.99/6	1.97/2
								1.96/3
1.9056	978	26.5	3953	33.0		1.91/2		
1.8690	586	15.9	1952	16.3		1.88/2		
					1.77/2			
1.7590	290	7.9	1160	9.7	1.74/3			
1.7298	479	13.0	2154	18.0				
1.6733	541	14.7	2332	19.5	1.68/3			
1.6206	495	13.4	1413	11.8			1.63/2	
1.5994	269	7.3	1094	9.1		1.60/1		
1.5782	147	4.0	594	5.0				
1.5566	91	2.5	334	2.8				
1.5203	211	5.7	1250	10.4				
1.4672	51	1.4	207	1.7				
1.4359	266	7.2	1711	14.3				
1.4157	381	10.3	1308	10.9			1.41/1	
1.4044	300	8.1	922	7.7				
1.3525	155	4.2	729	6.1				
1.3402	339	9.2	2281	19.1				
1.3017	396	10.7	1728	14.4				
1.2569	1756	47.6	6387	53.4			1.26/1	
1.2449	214	5.8	1019	8.5				
1.2310	180	4.9	730	6.1				
1.1959	60	1.6	267	2.2				
1.1760	425	11.5	2197	18.4				
1.1487	1372	37.2	5233	43.7			1.15/1	
1.1242	203	5.5	1231	10.3				
1.1022	401	10.9	1589	13.3				

MN_3_5M, dried in dark, light, black area

d(≈)	Height	H%	Area	A%	Cinnabar	Calcite	Halite
5.2162	86	5.7	344	6.4			
3.8537	135	9.0	372	6.9		3.85/1	
3.7402	41	2.8	167	3.1			
3.3496	1381	92.0	5357	100.0	3.36/X		
							3.26/1
3.1562	261	17.4	827	15.4	3.17/3		
3.0285	466	31.0	1528	28.5		3.04/X	
2.8594	1342	89.4	4572	85.4	2.86/X		
							2.82/X
2.4868	106	7.0	289	5.4		2.49/1	
2.3662	91	6.1	369	6.9			
2.2804	277	18.4	695	13.0		2.28/2	
2.1767	42	2.8	176	3.3			
2.0713	443	29.5	1360	25.4	2.07/3	2.09/2	
2.0235	109	7.3	232	4.3			
1.9879	1079	71.9	4590	85.7	1.98/4		1.99/6
1.9083	354	23.6	1292	24.1		1.91/2	
1.8730	469	31.2	1178	22.0		1.88/2	
1.8197	51	3.4	267	5.0			
1.7631	172	11.5	305	5.7	1.77/2		
1.7330	660	43.9	1895	35.4	1.74/3		
1.6775	767	51.0	2806	52.4	1.68/3		
1.6255	538	35.8	1167	21.8			1.63/2
1.6033	204	13.6	588	11.0		1.60/1	
1.5821	103	6.9	243	4.5			
1.5227	155	10.3	935	17.5			
1.5070	58	3.9	248	4.6			
1.4706	73	4.8	196	3.7			
1.4305	220	14.6	837	15.6			
1.4082	239	15.9	607	11.3			1.41/1
1.3720	36	2.4	167	3.1			
1.3566	149	9.9	817	15.2			
1.3431	578	38.5	2828	52.8			
1.3044	606	40.3	2124	39.6			
1.2673	220	14.6	1050	19.6			
1.2592	1502	100.0	5188	96.8			1.26/1
1.2474	272	18.1	1139	21.3			
1.1994	53	3.5	219	4.1			
1.1788	397	26.4	1658	31.0			
1.1504	948	63.1	2903	54.2			1.15/1
1.1260	293	19.5	1676	31.3			
1.1194	221	14.7	1150	21.5			
1.1040	503	33.5	1741	32.5			
1.0816	251	16.7	1040	19.4			

References

Arendt, Claus. 1991. “The Role of Architectural Fabric in the Preservation of Wall Paintings.” *The Conservation of wall paintings: proceedings of a symposium organized by the Courtauld Institute of Art and the Getty Conservation Institute, London, July 13-16, 1987*. Ed. Sharon Cather. Marina del Rey, CA: Getty Conservation Institute.

Arnold, Andreas and Kornad Zehnder. 1991. “Monitoring Wall Paintings Affected by Soluble Salts.” *The Conservation of wall paintings: proceedings of a symposium organized by the Courtauld Institute of Art and the Getty Conservation Institute, London, July 13-16, 1987*. Ed. Sharon Cather. Marina del Rey, CA: Getty Conservation Institute.

Ausset, P., R. Lef.vre, J. Philippon, and C. Venet. 1992. “Large-scale distribution of fly-ash particles inside weathering crusts on calcium carbonate substrates: Some examples on French monuments.” In La *conservation des monuments dans le basin méditerranéen: Actes du 2ème symposium international = The Conservation of Monuments in the Mediterranean Basin: Proceedings of the 2nd International Symposium, ed. D. Decrouez, J. Chamay, and F. Zezza, 121–39.* Geneva: Ville de Gen.ve, Mus.um d’histoire naturelle, and Muse d’art et d’histoire.

Barta, C. , J. Bryknar, Z., and M. Procio. 1987. "Photosensitivity of mercurous chloride single crystals in 280–400 nm spectral region." *Czechoslovak Journal of Physics B.* 37(11): 1301-1310.

Béarat, H. 1996. “Chemical and mineralogical analyses of Gallo-Roman wall painting from Dietikon, Switzerland.” *Archaeometry,* 38(1): 81-95.

Béarat, H., A. Chizmeshya, R. Sharma, A. Barbet, M. Fuchs. 2013. “Mechanistic and computational study of cinnabar phase transformation: Applications and implications to the preservation of this pigment in historical painting.” *The 3rd International Conference on Science and Technology in Archaeology and Conservation*, 7-11.

Bussagli, Marco. 1999. *Rome, Art and Architecture*. Cologne: Könemann.

Charola, A. E., Pühringer, J., & Steiger, M. 2007. “Gypsum: a review of its role in the deterioration of building materials.” *Environmental Geology*, *52*(2): 339-352.

Charola, A. E., and R. Ware. 2002. “Acid deposition and the deterioration of stone: A brief review of a broad topic.” In *Natural Stone, Weathering Phenomena, Conservation Strategies and Case Studies,* Ed. S. Siegesmund, T. Weiss, and A. Vollbrech. Geological Society Special Publications 205. London: Geological Society of London, 393–406.

Ciferri, Orio, Piero Tiano, and Giorgio Mastromei. 2000. *Of microbes and art: the role of microbial communities in the degradation and protection of cultural heritage*. New York: Kluwer Academic/Plenum Publishers.

Clarke, John R. 1991. *The houses of Roman Italy, 100 B.C.-A.D. 250: Ritual, Space, and Decoration*. Berkeley: University of California Press.

Cotte, Marine, Jean Susini, Nicole Metrich, Alessandra Moscato. 2006. "Blackening of Pompeian Cinnabar Paintings: X-ray Microspectroscopy Analysis." *Analytical Chemistry. 78*(21): 7484-7492.
Cotte, Marine, Jean Susini, V. Armando Solâe, Yoko Taniguchi, Javier Chillida, Emilie Checroun, and Philippe Walter. 2008. "Applications of synchrotron-based micro-imaging techniques to the chemical analysis of ancient paintings". *Journal of Analytical Atomic Spectrometry.* 23(6): 820-828.

Cotte, M., and J. Susini. 2009. "Watching Ancient Paintings through Synchrotron-Based X-Ray Microscopes". *MRS Bulletin.* 34(6): 403.

Cotte M., Susini J., Dik J., and Janssens K. 2010. "Synchrotron-based X-ray absorption spectroscopy for art conservation: Looking back and looking forward". *Accounts of Chemical Research.* 43(6): 705-714.

Daniels, V. 1987. The Blackening of Vermillion by Light. In *Recent Advances in Conservation and Analysis of Arifacts*. Ed. J. Black. Summer School Press: London, 833-835.

Daniels, V., R. Stacey, and A. Middleton. 2004. "The Blackening of Paint Containing Egyptian Blue". *Studies in Conservation.* 49: 217-230.

Davidson, R. S. and C.J. Willsher. 1981. “The Light-induced Blackening of Red Mercury (II) Sulphide.” *Journal of the Chemical Society, Dalton Transactions* 3: 833-835.

Davidson, R. Stephen, Charles J. Willsher, and Colin L. Morrison. 1982. "Influence of some solvents and solutes on illuminated red mercury(II) sulphide electrodes". *Journal of the Chemical Society, Faraday Transactions 1.* 78 (4): 1011-1019.

Dei, Luigi, Andreas Ahle, Piero Baglioni, Daniela Dini, and Enzo Ferroni. 1998. "Green degradation products of azurite in wall paintings: identification and conservation treatment." *Studies in Conservation.* 43(2): 80-88.

Dickson, F. W. and G. Tunell. 1959. “The Stability of Cinnabar and Metacinnabar.” *The American Minerologist.* 44: 471-487.

Doehne, Eric Ferguson, and C. A. Price. 2010. *Stone Conservation: An Overview of Current Research*. Los Angeles, Calif: Getty Conservation Institute.

Dreyer, R. M. 1938. Darkening of Cinnabar in Sunlight. *American Mineralogist*. 23: 796-798.

Fassina, V. 1992. “Atmospheric pollutants responsible for stone decay: Wet and dry surface deposition of air pollutants on stone and the formation of black scabs.” In *Weathering and Air Pollution: Primo corso della Scuola universitaria C.U.M. conservazione dei monumenti, Lago di Garda (Portese), Venezia, Milano, 2–9 Settembre 1991*. Ed. F. Zezza. Bari: Mario Adda Editore, 67-86.

Feller, R. L. 1967. “Studies on the Darkening of Vermilion by Light.” *Report and Studies in the History of Art*. National Gallery of Art, Washington, DC.

Gauri, K. Lal, Ahad N. Chowdhury, Niraj P. Kulshreshtha, and Adinarayana R. Punuru. 1989. "The sulfation of marble and the treatment of gypsum crusts." *Studies in Conservation.* 34(4): 201-206.

Gerbig, C.A., Kim, C.S., Stegemeier, J.P., Ryan, J.N., Aiken, G.R., 2011. “Formation of Nanocolloidal Metacinnabar in Mercury-DOM-Sulfide Systems” *Environmental Science & Technology.* 45: 9180-9187.

Gettens, R.J., Feller, R.L., Chase, W.T. 1993. “Vermilion and Cinnabar.” In *Artists Pigments, Vol. 2*. Ed. A. Roy. Oxford University Press: New York, 167-168.
_____. 1986. “Vermillion and cinnabar,” In *Artists' pigments a handbook of their history and characteristics*. Ed. Feller, Robert L., Ashok Roy, Elisabeth West FitzHugh, and Barbara Hepburn Berrie. Washington: National Gallery of Art.
_____. 1972. Vermilion and Cinnabar, “Studies in Conservation. 17:45–69.

Gettens, R.J and G. L. Stout. 1966. *Painting Materials: A short Encyclopaedia*, New York: Dover Publications.

Giovannoni, Sabino, Mauro Matteini, and Arcangelo Moles. 1990. "Studies and Developments Concerning the Problem of Altered Lead Pigments in Wall Painting." *Studies in Conservation.* 35: 33-51.

Grout, R., Burnstock, A., 2000. “A study of the blackening of vermilion.” *Zeitschrift für Kunsttechnologie und Konservierung*. 141: 15-22.

Hsieh, Y. H., S. Tokunaga, C.P. Huang. 1991. “Some chemical reactions at the HgS(s)—water interface as affected by photoirradiation.” *Colloids and Surfaces*. 53(2): 257-274.

Istudor, I., A. Dina, G. Rosu, D. Seclaman and G. Niculescu. 2007. “An Alteration Phenomenon of Cinnabar Red Pigment in Mural Paintings from Sucevita.” *E_Conservation.* 2: 24-33.

Johnston-Feller, Ruth. 2001. *Color science in the examination of museum objects nondestructive procedures.* Los Angeles: Getty Conservation Institute.

Kakoulli I. and Fischer C. 2009. “An innovative noninvasive and nondestructive multidisciplinary approach for the technical study of the Byzantine wall paintings in the Enkleistra of St. Neophytos in Paphos, Cyprus.” *Project Grant Reports*, Dumbarton Oak.

Keune, Katrien, and Jaap J. Boon. 2005. "Analytical Imaging Studies Clarifying the Process of the Darkening of Vermilion in Paintings". *Analytical Chemistry.* 77(15): 4742-4750.

Kulik, D., Berner, U., Curti, E. 2003. Modelling chemical equilibrium partitioning with the GEMS-PSI code. *PSI Scientific Report, http://gems.web.psi.ch.* 4: 109-122.

Lehmann, Phyllis Williams. 1953. *Roman wall paintings from Boscoreale in the Metropolitan Museum of Art*. Cambridge: Archaeological Institute of America.

Ling, Roger. 1991. *Roman Painting*. Cambridge: Cambridge University Press.

Litter, M. I. 1999. "Heterogeneous photocatalysis - Transition metal ions in photocatalytic systems". *Applied Catalyst B.* 23(2-3): 89-114.

Maiuri, Amedeo. 1953. *Roman Painting.* Trans. Stuart Gilbert. Skira: Geneva.

Matteini, Mauro. 1991. "In Review: An Assessment of Florentine Methods of Wall Painting Conservation Based on the Use of Mineral Treatments." *The Conservation of wall paintings: proceedings of a symposium organized by the Courtauld Institute of Art and the Getty Conservation Institute, London, July 13-16, 1987*. Ed. Sharon Cather. [Marina del Rey, CA]: Getty Conservation Institute.

McCormack, J. K. 2000. "The darkening of cinnabar in sunlight". *Mineralium Deposita*. 35: 796-798
_____. 1997. Mercury sulf-halide minerals and crystalline phases, and experimental formation conditions, in the system $Hg_3S_2Cl_2$-$Hg_3S_2Br_2$-$H_3S_2I_2$. Thesis (Ph. D.)--University of Nevada, Reno.

McCormak, J. K. and F. W. Dickerson. 1998. "Polymorphism, solid solutions and structural similarities of Mercury Sulfhalide Minerals and Solid Phases." *Abstracs of the Eos of American Geo-physical Union Fall Meeting in San Francisco*. Supp 79: F1016.

McCormack, John K., Frank W. Dickson, and Maureen P. Leshendok. 1991. "Radtkeite, Hg 3 S 2 ClI, a new mineral from the McDermitt mercury deposit, Humboldt County, Nevada." *American Mineralogist.* 76(9-10): 1715-1721.

Minopoulou, E. 2009. "A Study of Smalt and Red Lead Discolouration in Antiphonitis Wall Paintings in Cyprus". *Applied Physics Materials Science and Processing.* 96(3): 701-711.

Moormann, Eric M. 1993. *Functional and Spatial Analysis of Wall Painting: Proceedings of the Fifth International Congress on Ancient Wall Painting, Amsterdam, 8-12 September 1992*. Leiden: Stichting Babesch.

Mora, Paolo, Laura Mora, and Paul Philippot. 1984. *The Conservation of Wall Paintings*. New York: Butterworth & Co.

Okouchi, S, and S Sasaki. 1983. "Photochemical behavior of mercury ore in water". *Environment International.* 9(2): 103-106.

Pal B, S Ikeda, and B Ohtani. 2003. "Photoinduced chemical reactions on natural single crystals and synthesized crystallites of mercury(II) sulfide in aqueous solution containing naturally occurring amino acids". *Inorganic Chemistry.* 42(5): 1518-24.

Parks, G. A and D. K Nordstrom. 1979. "Estimated free energies of formation, water solubilities,

and stability fields for schuetteite (Hg3O2SO4) and corderoite (Hg3S2Cl2) at 298 K." *Chemical Modeling in Aqueous Systems*. 93: 339-352.

Perez-Alanso, M., K Castro, M. Alvarez and J. M. Madariaga. 2006. "Investigation of Degredation Mechanisms by Progable Raman spectroscopy and Therodunamic Speciation: The Wall Paining of Santa Maria de Lemoniz (Basque County, North of Spain)," *Analytica Chimica Acta*. 571: 121-128.

Piqué, F. 2007. "Indagini non invasive sulle pitture del Tablino nella Casa del Bicentenario a Ercolano." Materiali e Strutture. 9-10: 6-27.

Pliny. 1929. *The Elder Pliny's Chapters on Chemical Subjects*. Ed. Kenneth C. Bailey. London: E. Arnold & Co.

Radepont, Marie, Wout de Nolf, Koen Janssens, Geert Van der Snickt, Yvan Coquinot, Lizet Klaassen, and Marine Cotte. 2011. "The use of microscopic X-ray diffraction for the study of HgS and its degradation products corderoite, kenhsuite and calomel in historical paintings". *Journal of Analytical Atomic Spectrometry.* 26(5): 959-968.

Radepont, Marie, Marine Cotte, and Koen Janssens. 2013. *Understanding of chemical reactions involved in pigment discoloration, in particular in mercury sulfide (HgS) blackening*. PhD diss, Universiteit Antwerpen.

Schweppe, H., J. Winter. 1997. "Vermilion and Cinnabar." In *Artists Pigments Vol. 3.* Ed. West FitzHugh. New York: Oxford University Press.

Spring, Marika and Rachel Grout. 2002. "The Blackening of Vermilion: An Analytical Study of the Process in Paintings." *The National Gallery Technical Bulletin*. 23 (1): 50-61.

Sotiropoulou, S., et al., 2008. "*Microanalytical investigation of degradation issues in Byzantine wall paintings." Applied Physics A: Materials Science & Processing*. 92(1):43-150.

Stratoudaki, T., A. Manousaki, K. Melesanaki, V. Zafiropulos, and G. Orial. 2010. "Study on the discolouration of pigments induced by laser irradiation". *Revue De Métallurgie. Cahiers D'informations Techniques.* 9: 795.

Stromberg, D., A. Stromberg, and U. Wahlgren. 1991. "Relativistic Quantum Calculations on Some Mercury Sulfide Molecules". *Water, Air, and Soil Pollution.* 56: 681-696.

Tennikat, Manuela. 1994 "Blumenkohl-, Sinter-und Seidenglanzkruste: Salzkartierung und naturwissenschaftliche Erklärungen." *Forschungsprojekt Wandmalerei-Schäden: ein Förderprojekt des Bundesministers für Forschung und Technologie: Schlußbericht zu den interdisziplinären Befunden*. Niedersächsisches Landesverwaltungsamt, 99-108.

Terzano, R., Santoro, A., Spagnuolo, M., Vekemans, B., Medici, L., Janssens, K., GѴðttlicher, J.r., Denecke, M.A., Mangold, S., Ruggiero, P. 2010. "Solving mercury (Hg) speciation in soil samples by synchrotron X-ray microspectroscopic techniques." Environmental Pollution. 158: 2702-2709.

Toniolo, L., C. M. Zerbi, and R. Bugini. 2009. Black layers on historical architecture." *Environmental Science and Pollution Research.* 16(2): 218–26.

Vitruvius. 1960. *The Ten Books on Architecture.* Tran. H. M. Morgan. New York: Dover Publications.